

# UC San Diego

## UC San Diego Previously Published Works

### Title

Modeling of electrochemomechanical response of ionic polymer-metal composites with various solvents

### Permalink

<https://escholarship.org/uc/item/12r2m1tk>

### Journal

Journal of Applied Physics, 100(6)

### ISSN

0021-8979

### Authors

Nemat-Nasser, S  
Zamani, S

### Publication Date

2006-09-01

Peer reviewed

## Modeling of electrochemomechanical response of ionic polymer-metal composites with various solvents

Sia Nemat-Nasser<sup>a)</sup> and Shahram Zamani

*Center of Excellence for Advanced Materials, Department of Mechanical and Aerospace Engineering, University of California, San Diego, 9500 Gilman Drive, La Jolla, California 92093-0416*

(Received 18 October 2005; accepted 5 June 2006; published online 22 September 2006)

Ionic polymer-metal composites (IPMCs) consist of a perfluorinated ionomer membrane (usually Nafion<sup>®</sup> or Flemion<sup>®</sup>) plated on both faces with a noble metal such as gold or platinum and neutralized with the necessary amount of counterions that balance the electrical charge of anions that are covalently fixed to the backbone ionomer. IPMCs are electroactive materials with potential applications as soft actuators and sensors. Their electrical-chemical-mechanical response is dependent on the cations used, the nature and the amount of solvent uptake, the morphology of the electrodes, the composition of the backbone ionomer, the geometry and boundary conditions of the composite element, and the magnitude and spatial and temporal variations of the applied potential. Our most recent experimental results show that solvents can have profound effects on the nature of the IPMCs' actuation. For example, we have discovered experimentally that Nafion-based IPMCs in Li<sup>+</sup>-form show very small back relaxation when hydrated, but extensive back relaxation with all other solvents that we have considered. On the other hand, the same membrane in the K<sup>+</sup>-form has extensive back relaxation when solvated with water, ethylene glycol, or glycerol, but none with 18-Crown-6. In the present paper, we seek to model the IPMCs' actuation and compare results with the experimental data. The modeling rests on the observation that a sudden application of a step potential (dc) of several volts (1–3 V) alters the distribution of cations within the ionomer, forcing cations out of the clusters near the anode and additional cations into the clusters near the cathode. The clusters within a thin boundary layer near the anode are thus depleted of their cations, while cations accumulate in the clusters near the cathode boundary layer. We first seek to determine the spatial and temporal variations of the cation distribution across the thickness of the IPMC for various cations and solvents, using an implicit finite difference numerical solution of the basic field equations, and compare the results with those of approximate analytical estimates. Based on this information, we then calculate the changes in the osmotic, electrostatic, and elastic forces that tend to expand or contract the clusters in the anode and cathode boundary layers. Finally, we calculate the amount of solvent out of or into the clusters that produces the bending motion of the cantilever. Comparing the model results with those of experimental measurement, we have arrived at remarkably good agreements. Indeed, our nanoscale-based model correctly predicts the unexpected influence of solvents on the actuation of IPMCs. © 2006 American Institute of Physics. [DOI: 10.1063/1.2221505]

### I. INTRODUCTION

Ionic polymer-metal composites (IPMCs) are electroactive materials with potential applications as actuators and sensors.<sup>1</sup> When a cantilevered IPMC sample is subjected to a suddenly applied potential (dc) of several volts (1–3 V), the electric field alters the distribution of cations within the ionomer, forcing them to move from the anode towards the cathode. The clusters within a thin boundary layer near the anode are thus depleted of their cations, while cations accumulate in the clusters near the cathode boundary layer. The distribution of cations under an applied potential may be modeled using the Nernst-Planck equation to define the flux of species under electrochemical potential diffusion and the Poisson equation to relate the concentration of species to the electric

field. In this manner the approximate analytical solution of Nemat-Nasser<sup>2</sup> can be checked and improved, arriving at a better prediction of the experimentally observed cation transfer as a function of time.

An efficient computer algorithm has been developed<sup>3</sup> for numerical simulation of membrane transport based on the Nernst-Planck and Poisson equations, and using an implicit finite-difference method. In this work, we follow a similar methodology and find the spatial and temporal variations of cations within an IPMC sample that is subjected to an electric potential. Then, based on the knowledge of the cation imbalance within the clusters (but not in the IPMC), we calculate the changes in the osmotic, electrostatic, and elastic forces that tend to expand or contract the corresponding clusters. From this we calculate the amount of solvent out of or into the clusters, and predict the resulting bending motion of the cantilever.

<sup>a)</sup>Electronic mail: sia@ucsd.edu

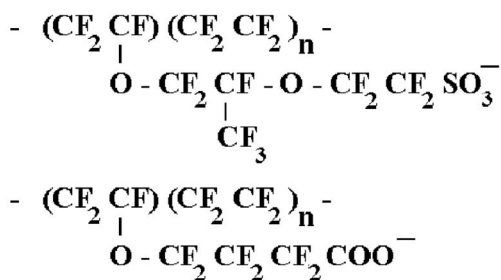


FIG. 1. Chemical structure of Nafion (top) and Flemion (bottom).

## II. MICROSTRUCTURE AND PROPERTIES

### A. Composition and properties

IPMCs are electroactive materials with potential applications as actuators and sensors.<sup>1</sup> An IPMC consists of a perfluorinated backbone ionomer [usually Nafion<sup>®</sup> or Flemion<sup>®</sup>;  $(\text{CF}_2\text{CF})_m(\text{CF}_2\text{CF}_2)_n$ ; see Fig. 1] plated on both faces with noble metals such as platinum, platinum and gold, or gold, and neutralized with the necessary amount of counterions that balance the electric charge of the anions covalently bonded to the ionomer.<sup>4</sup> The electrical-chemical-mechanical response of the IPMCs depends on the neutralizing cation, the nature of the solvent and its degree of saturation, the electrode morphology, and the chemical structure and characteristics of the backbone ionomer.

### B. Actuation of IPMCs

When a thin strip of an IPMC membrane in the solvated state is subjected to a suddenly imposed and sustained constant electric potential (dc) of several volts (1–3 V), it bends towards the anode. For Nafion-based IPMCs that are neutralized with alkali metal cations and solvated by water, ethylene glycol, or glycerol, the strip then slowly relaxes back towards the cathode, while still under electric potential.<sup>2,4–6</sup> The sample eventually reaches an equilibrium state (while the electric potential is still on), which is generally far from its initial equilibrium position. If the electric potential is removed as the two electrodes are shorted, the Nafion-based IPMC sample (under the above-mentioned conditions) displays a relatively fast bending deformation towards the cathode and then slowly relaxes back towards the anode, seldom attaining its initial state. Experimental observations<sup>7</sup> for Flemion-based IPMCs show that the initial actuation towards the anode is followed by slower relaxation in the same (i.e., towards the anode) direction. Hence, unlike Nafion-based IPMCs no back relaxation has been detected for Flemion-based IPMCs, in experiments conducted so far.

Thus, with water, ethylene glycol, or glycerol as solvents, the actuation of the Nafion-based IPMCs has essentially the same qualitative character, the basic difference being the speed of actuation which directly correlates with solvent viscosity. With crown ethers, on the other hand, we discovered experimentally<sup>6</sup> that there may be a remarkable qualitative change in the actuation, depending on the cation and the crown ether. For example, Nafion-based IPMCs in Li<sup>+</sup>-form show only a small relaxation towards the cathode

with water, but with ethylene glycol, glycerol, or 12-Crown-4 they show extensive back relaxation towards the cathode after an initial small actuation towards the anode. In the K<sup>+</sup>-form, on the other hand, the Nafion-based IPMC shows extensive back relaxation for water, ethylene glycol, or glycerol, but no backward relaxation for the 18-Crown-6, for which the relaxation is then in the direction of the initial actuation, namely, towards the anode. Similarly, back relaxations are observed for Na<sup>+</sup>-form IPMCs with water, ethylene glycol, glycerol, and 18-Crown-6, but not with 15-Crown-5 as solvent. In the case of 18-Crown-6, the initial bending towards the anode is followed by back relaxation towards the cathode, as occurs (at different speeds) when water, ethylene glycol, or glycerol is used for the solvent. Our nanoscale model correctly predicts all these results, as is summarized and illustrated in this paper.

### C. Micro-mechanisms of Actuation

The basic idea underpinning the actuation modeling is that the application of an electric potential produces two thin boundary layers, one near the anode and the other near the cathode electrodes. As a result, the clusters in the anode boundary layer are gradually depleted of their cations, while those in the cathode boundary layer are gradually supplied with additional cations. The cation imbalance within the clusters (but not in the IPMC) changes the osmotic, electrostatic, and elastic forces that tend to expand or contract the corresponding clusters, forcing the solvents out of or into the clusters, and thus produces the bending motion of the cantilever. Therefore, in this model, the volume fraction of the solvent within each boundary layer is assumed to be controlled by the effective pressure in the corresponding clusters produced by the osmotic, electrostatic, and elastic forces.

### D. Some basic characteristic parameters

An important parameter that characterizes an ionomer is its ion content, defined by

$$EW_{\text{ion}} = \frac{EW_{\text{H}^+} - 1.008 + FW_{\text{ion}}}{SF}, \quad (1)$$

where  $EW_{\text{H}^+}$  is the equivalent weight of dry Nafion polymer in H<sup>+</sup>-form, which for Nafion 117 is almost 1100 g/mol (ion exchange capacity of  $1/1100=0.99$  meq g<sup>-1</sup>).  $FW_{\text{ion}}$  is the formula weight of the cation used, and  $SF$  accounts for the metal plating, being the ratio of the dry backbone polymer mass to the total mass of the IPMC sample. For the bare polymer (no metal plating),  $SF=1$ .

Another characteristic of a solvated sample is the solvent uptake that affects both the stiffness and the actuation behavior of the material. Solvent uptake is defined as the ratio of the volume of the absorbed solvent to the volume of the dry IPMC sample,

$$w = \frac{V_s}{V_d} = \frac{1}{\rho_s V_d} (m_{\text{total}} - m_d), \quad (2)$$

where  $V_s$  is the volume of the absorbed solvent,  $V_d$  is the volume of the dry sample,  $\rho_s$  is the density of the solvent,

$m_{\text{total}}$  is the total mass of the sample in the solvated form, and  $m_d$  is the mass of the dry sample.

The concentration of anions in the bare membrane,  $C^-$ , is the number of anions (in mole) per unit volume (in  $\text{cm}^3$ ) of the solvated sample, defined by

$$C^- = \frac{\rho_d}{EW_{\text{ion}}} \frac{1}{1+w}, \quad (3)$$

where  $\rho_d$  is the dry density of the IPMC sample.

### III. MODELING OF STIFFNESS VERSUS SOLVATION

A dry sample of a bare polymer or an IPMC in a solution absorbs the solvent until the resulting pressure within the clusters is balanced by the elastic stresses that are consequently developed within its backbone polymer membrane. From this observation, we calculate the stiffness of the membrane as a function of the volume fraction of the solvent uptake for various cations. We first consider the balance of cluster pressure and elastic stresses for the bare polymer (no metal plating) to calculate the stiffness of the bare membrane for a given solvent uptake. Then we use the results to calculate the stiffness of the corresponding IPMC by including the effect of the added metal electrodes. The procedure also provides a way of estimating the microstructural parameters that are needed for modeling the actuation of IPMCs. For Nafion-based IPMCs, the overall stiffness of both the bare membrane and the corresponding IPMC has been measured directly as a function of the degree of solvation. Therefore, the results can be subjected to experimental verification.

The pressure developed within the cluster,  $p_c$ , can be shown<sup>2</sup> to be given by

$$p_c = \frac{\nu Q_B^- K_0 \phi}{w} + \frac{1}{3\kappa_e} Q_B^- \frac{2\pm\alpha^2}{w^2}, \quad K_0 = \frac{RT}{F}, \quad Q_B^- = \frac{\rho_B F}{EW_{\text{ion}}}, \quad (4)$$

where  $\phi$  is the practical osmotic coefficient,  $\alpha$  is the effective length of the dipole,  $F$  is the Faraday constant,  $\nu$  is the cation-anion valence ( $\nu=2$  for monovalent cations),  $R=8.314$  J/mol/K is the universal gas constant,  $T=300$  K is the test (room) temperature,  $\rho_B$  is the density of the bare ionomer, and  $\kappa_e$  is the effective permittivity. Furthermore, from the balance of the elastic resistance of the membrane against the cluster expansion and the cluster pressure, it is shown that the stiffness,  $K(w)$ , of the bare polymer can be estimated as follows:<sup>2</sup>

$$K = p_c \frac{1+w}{w_0 I_n - (w_0/w)^{4/3}},$$

TABLE I. Refractive index  $n$  and dipole moment  $\mu_m$  of water, glycerol, and ethylene glycol at room temperature (Ref. 9).

	Water	Glycerol	Ethylene glycol
$n$	1.334	1.474	1.383
$\mu_m$ (D)	1.90	2.56	2.36

$$I_n = \frac{1+2An_0}{n_0(1+An_0)^{1/3}} - \frac{1+2A}{(1+A)^{1/3}}, \quad (5)$$

$$A = \frac{w}{w_0} - 1,$$

where  $n_0$  and  $w_0$  are the initial (dry) porosity and initial void ratio, respectively. The IPMC stiffness,  $\bar{Y}_{\text{IPMC}}$ , is now given by

$$\bar{Y}_{\text{IPMC}} = \frac{Y_M Y_B}{BA_B Y_M + (1-BA_B) Y_B}, \quad (6)$$

$$B = \frac{(1+\bar{w})(1-f_M)}{1+\bar{w}(1-f_M)}, \quad \bar{w} = w(1-f_M)^{-1},$$

$$f_M = \frac{(1-\text{SF})\rho_B}{(1-\text{SF})\rho_B + \text{SF}\rho_M}, \quad (7)$$

where  $f_M$  is the volume fraction of the metal plating in a dry sample,  $Y_M$  and  $Y_B$  are Young's moduli of the metal plating and bare ionomer, respectively,  $\rho_M$  is the density of the metal plating, and  $A_B$  is the concentration factor that accounts for the contribution of the bare ionomer in carrying the average overall stress within the sample.

To estimate  $\kappa_e$ , the effective cluster electric permittivity, as a function of the solvent uptake  $w$ , note that solvent molecules are polar. As part of the solvation shell of an ion, a polar solvent has a dielectric constant of, say,  $\epsilon_1$ , whereas as free molecules its dielectric constant is much larger, say,  $\epsilon_2$ , both at room temperature. To estimate the solvent dielectric constants in bulk and as a part of the solvation shell, we use the following equation:<sup>8</sup>

$$\epsilon E = \frac{4\pi}{M_{\text{solvent}}} \frac{n^2+2}{3} L \left( \frac{n^2+2}{2} \frac{\mu_m E}{kT} \right) + \frac{3}{2}(n^2-1)E, \quad (8)$$

where  $M_{\text{solvent}}$  is the solvent's molecular weight,  $n$  is its refractive index,  $E$  is the applied electric field,  $\mu_m$  is the dipole moment,  $k$  is Boltzmann's constant, and  $L$  is the Langevin function defined by

$$L(y) = \coth(y) - \frac{1}{y}. \quad (9)$$

The refractive index  $n$  and the dipole moment  $\mu_m$  of the solvents under study are given in Table I; data from Ref. 9. The calculated dielectric constants are shown in Table II.

To find the number of moles of cations within a given sample of bare ionomer, we use the measured solvent uptake  $w$ , sample length  $L$ , width  $w_d$ , thickness  $2H$ , and its dry density  $\rho_d$ . For example, for a sample in  $\text{K}^+$ -form with  $\text{FW}_{\text{ion}}=39$  g/mol,  $w=1.47$ ,  $L=2.6982$  cm,  $w_d=0.2509$  cm,

TABLE II. Calculated dielectric constant in bulk and as a part of the solvation shell of an ion for various solvents using Eq. (8).

	Water	Glycerol	Ethylene glycol
$\epsilon_1$	6.2	9.4	7.7
$\epsilon_2$	78.4	46.5	41.0

$2H=0.0178$  cm (resulting in  $1.18 \times 10^{-8}$  cm<sup>3</sup> for volume), and  $\rho_d=2.07$  g/cm<sup>3</sup>, the cation content in moles then is

$$x_C = \left( \frac{\rho_d}{EW_{\text{ion}}} \frac{1}{1+w} \right) (1+w)V_d = 2.15 \times 10^{-5}. \quad (10)$$

In the solution of 4.2 g of 18CR6 ( $m_{18\text{CR}6}=4.2$  g) and 10 ml of glycerol ( $V_G=10$  ml) (see Nemat-Nasser *et al.*<sup>6</sup> for details on preparation of the crown ether solutions), the moles of glycerol,  $x_G$ , are given by

$$x_G = \frac{\rho_s V_G}{M_G} = 0.137, \quad (11)$$

where  $M_G$  represents the molecular weight of the glycerol. We calculate moles of crown, say,  $x_{18\text{CR}6}$ , to be

$$x_{18\text{CR}6} = \frac{m_{18\text{CR}6}}{M_{18\text{CR}6}} = 0.016. \quad (12)$$

Using (11) and (12), we obtain

$$\frac{x_G}{x_{18\text{CR}6}} = 9. \quad (13)$$

We assume that the same ratio holds in the backbone ionomer. The total weight change due to the solvation is given by

$$M_G x_G + M_{18\text{CR}6} x_{18\text{CR}6} = m_{\text{total}} - m_d. \quad (14)$$

Using Eq. (13), the moles of glycerol,  $y_G$ , and 18CR6,  $y_{18\text{CR}6}$ , within the sample are

$$y_G = 1.7 \times 10^{-4}, \quad y_{18\text{CR}6} = 1.9 \times 10^{-5}. \quad (15)$$

Then, the mole of solvent per mole of ion is

$$\frac{y_G}{x_C} \approx 8 \frac{\text{moles of glycerol}}{\text{mole of cation}}, \quad (16)$$

$$\frac{y_{18\text{CR}6}}{x_C} \approx 0.9 \frac{\text{moles of 18CR6}}{\text{mole of cation}}.$$

The above calculation shows that 90% of the cations is embraced by the crown ether. Therefore, the rest of the cations (10%) and all the anions are surrounded by the glycerol through their solvation shell. A similar procedure for 12CR4 and 15CR5 yields

$$\frac{y_G}{x_C} = 8 \frac{\text{moles of glycerol}}{\text{mole of cation}}, \quad (17)$$

$$\frac{y_{15\text{CR}5}}{x_C} = 0.9 \frac{\text{moles of 15CR5}}{\text{mole of cation}},$$

$$\frac{y_G}{x_C} = 8 \frac{\text{moles of glycerol}}{\text{mole of cation}}, \quad (18)$$

$$\frac{y_{12\text{CR}4}}{x_C} = 0.9 \frac{\text{moles of 12CR4}}{\text{mole of cation}}.$$

Let CN be the static solvation shell of the cation (which equals its corresponding coordination number),  $m_w$  be the number of moles of solvent per mole ion (cation and anion) within a cluster, and note that

$$m_w = \frac{EW_{\text{ion}} w}{M_{\text{solvent}} \rho_B \nu}. \quad (19)$$

We use  $\nu=2$  for water, ethylene glycol, and glycerol, but we use  $\nu=1.1$  for crown ether solutions, since, in those cases, only 10% of the cations are solvated by glycerol.

Hence, when the amount of solvent (in moles) per ion within a cluster is less than the coordination number CN of that ion, we set  $\kappa_e = \epsilon_1 \kappa_0$ , where  $\kappa_0 = 8.85 \times 10^{-12}$  F/m is the electric permittivity of free space. On the other hand, when  $m_w \geq \text{CN}$  then we calculate  $\kappa_e = \kappa_e(w)$  as follows (see Nemat-Nasser<sup>2</sup> for details):

$$\kappa_e = \frac{\kappa_2 + \kappa_1 + f(\kappa_2 - \kappa_1)}{\kappa_2 + \kappa_1 - f(\kappa_2 - \kappa_1)} \kappa_1, \quad \kappa_1 = \epsilon_1 \kappa_0, \quad (20)$$

$$\kappa_2 = \epsilon_2 \kappa_0, \quad f = \frac{m_w - \text{CN}}{m_w}.$$

To estimate the parameter  $\alpha^2$  in (4), first we assume that it varies linearly with  $w$  for  $m_w < \text{CN}$ , i.e., we set

$$\pm \alpha^2 = a_1 w + a_2, \quad (21)$$

and estimate the coefficients  $a_1$  and  $a_2$  from the experimental data using two measured values of the stiffness. The results are listed in Tables III–V. For  $m_w \geq \text{CN}$ , furthermore, we assume that the pseudodipole length is controlled by the electric permittivity of its environment, given by (in m<sup>2</sup>)

$$\alpha^2 = 10^{-20} \left( \frac{\kappa_e}{\kappa_1} \right)^2 (a_1 w + a_2). \quad (22)$$

TABLE III. Parameters, initial data, and other results used for stiffness modeling of bare Nafion ionomer and Nafion-based IPMC in Li<sup>+</sup>-form.

	Li <sup>+</sup>		
	EG	G	12CR4
FW <sub>ion</sub> (g/mol)	6.95	6.95	6.95
CN	6	6	3
$\epsilon_1$	7.7	9.4	9.4
$\epsilon_2$	41	46.5	46.5
$\rho_B$ (g/cm <sup>3</sup> )	2.01	2.01	2.01
$w$ (wet) (%)	85.0	83.8	70.3
$w$ (dry) (%)	3.8	4.1	3.5
$Y_B$ (wet) (MPa)	85	55	89
$Y_B$ (dry) (MPa)	756	611	630
$\phi$	1	1	1
$a_1$ (10 <sup>-20</sup> m <sup>2</sup> )	4.150	2.399	3.437
$a_2$ (10 <sup>-20</sup> m <sup>2</sup> )	-0.187	-0.166	-0.097
$A_B$	0.7	0.7	0.7

TABLE IV. Parameters, initial data, and other results used for stiffness modeling of bare Nafion ionomer and Nafion-based IPMC in Na<sup>+</sup>-form.

	Na <sup>+</sup>				
	W	EG	G	15CR5	18CR6
FW <sub>ion</sub> (g/mol)	23.0	23.0	23.0	23.0	23.0
CN	5	5	5	3	3
ε <sub>1</sub>	6	7.7	9.4	9.4	9.4
ε <sub>2</sub>	78	41	46.5	46.5	46.5
ρ <sub>B</sub> (g/cm <sup>3</sup> )	2.02	2.02	2.02	2.02	2.02
w (wet) (%)	47.5	146.1	53.8	70.0	120.0
w (dry) (%)	1.2	7.4	3.9	5.1	4.8
Y <sub>B</sub> (wet) (MPa)	92	40	65	75	40
Y <sub>B</sub> (dry) (MPa)	1363	388	600	455	485
φ	1	1	1	1	1
a <sub>1</sub> (10 <sup>-20</sup> m <sup>2</sup> )	1.728	1.853	1.340	2.692	2.031
a <sub>2</sub> (10 <sup>-20</sup> m <sup>2</sup> )	-0.071	-0.196	-0.116	-0.214	-0.033
A <sub>B</sub>	0.7	0.7	0.7	0.7	0.7

In a series of experiments, the extensional Young modulus  $Y_B$  of strips of bare Nafion in various cation forms has been measured as a function of the solvent uptake  $w$ . The solvated membrane is assumed to be incompressible. For small axial strains (i.e., less than 1%), therefore, the Young modulus  $Y_B$  of the solvated strip of bare polymer relates to the stiffness  $K$  by

$$Y_B = 3K. \tag{23}$$

Figures 2–13 show the experimentally measured Young’s modulus  $Y_B$  for Li<sup>+</sup>-, Na<sup>+</sup>-, and K<sup>+</sup>-form Nafion 117 ionomer with various solvents. In these figures, the results of the model are shown by solid curves. An initial porosity of  $n_0=0.01$  is used for the calculations. For crown ethers (last column of the tables), CN=3 represents the static solvation shell of sulfonate.<sup>9</sup>

TABLE V. Parameters, initial data, and other results used for stiffness modeling of bare Nafion ionomer and Nafion-based IPMC in K<sup>+</sup>-form.

	K <sup>+</sup>			
	EG	G	15CR5	18CR6
FW <sub>ion</sub> (g/mol)	39.1	39.1	39.1	39.1
CN	4	4	3	3
ε <sub>1</sub>	7.7	9.4	9.4	9.4
ε <sub>2</sub>	41	46.5	46.5	46.5
ρ <sub>B</sub> (g/cm <sup>3</sup> )	2.07	2.07	2.02	2.07
w (wet) (%)	32.0	42.8	133.0	83.8
w (dry) (%)	4.0	4.0	5.8	4.1
Y <sub>B</sub> (wet) (MPa)	148	80	45	85
Y <sub>B</sub> (dry) (MPa)	748	539	465	590
φ	1	1	1	1
a <sub>1</sub> (10 <sup>-20</sup> m <sup>2</sup> )	3.966	1.302	2.807	3.798
a <sub>2</sub> (10 <sup>-20</sup> m <sup>2</sup> )	-0.182	-0.150	-0.025	-0.233
A <sub>B</sub>	0.7	0.7	0.7	0.7

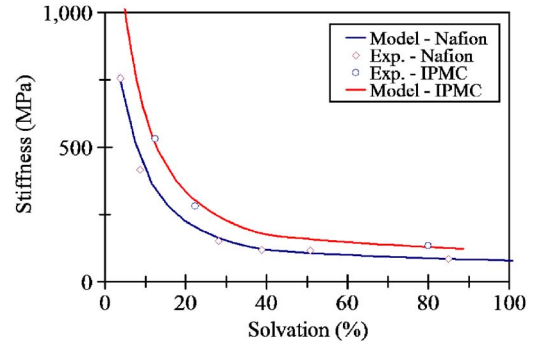


FIG. 2. Uniaxial stiffness (Young’s modulus) of bare Nafion 117 and IPMC (data points and the solid curve, model) in Li<sup>+</sup>-form vs solvation; ethylene glycol as solvent.

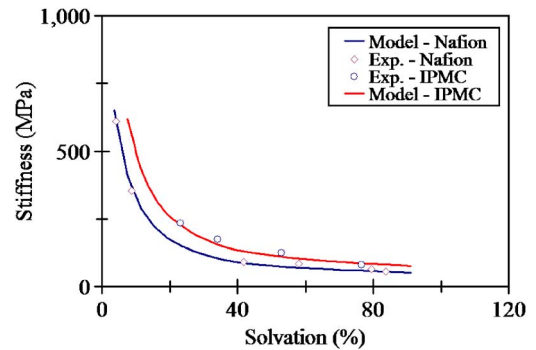


FIG. 3. Uniaxial stiffness (Young’s modulus) of bare Nafion 117 and IPMC (data points and the solid curve, model) in Li<sup>+</sup>-form vs solvation; glycerol as solvent.

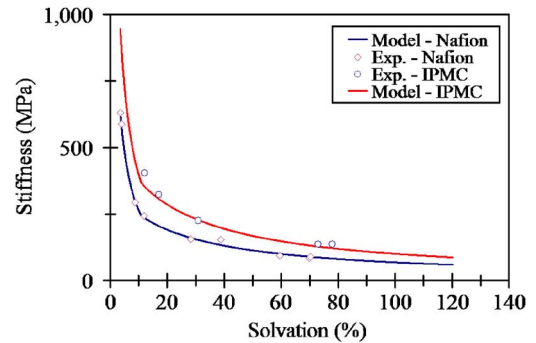


FIG. 4. Uniaxial stiffness (Young’s modulus) of bare Nafion 117 and IPMC (data points and the solid curve, model) in Li<sup>+</sup>-form vs solvation; 12-Crown-4 as solvent.

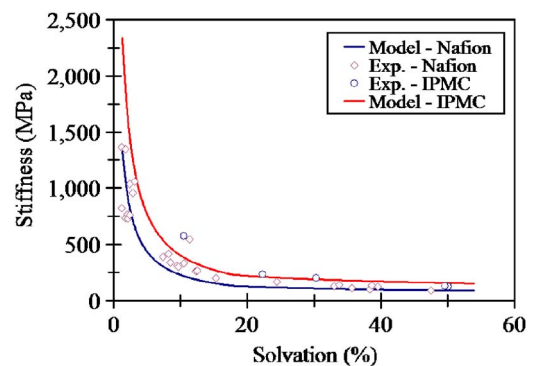


FIG. 5. Uniaxial stiffness (Young’s modulus) of bare Nafion 117 and IPMC (data points and the solid curve, model) in Na<sup>+</sup>-form vs solvation; water as solvent.

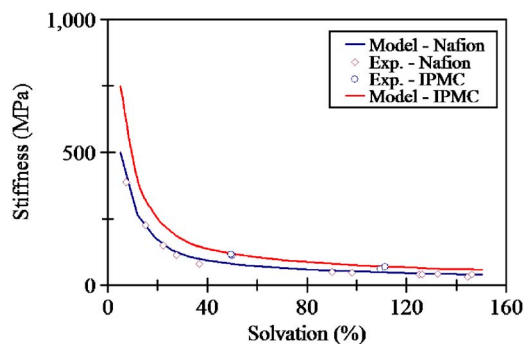


FIG. 6. Uniaxial stiffness (Young's modulus) of bare Nafion 117 and IPMC (data points and the solid curve, model) in Na<sup>+</sup>-form vs solvation; ethylene glycol as solvent.

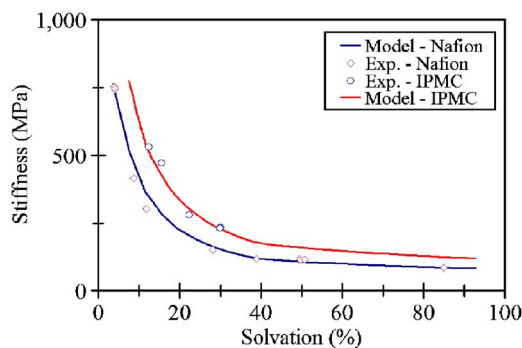


FIG. 10. Uniaxial stiffness (Young's modulus) of bare Nafion 117 and IPMC (data points and the solid curve, model) in K<sup>+</sup>-form vs solvation; ethylene glycol as solvent.

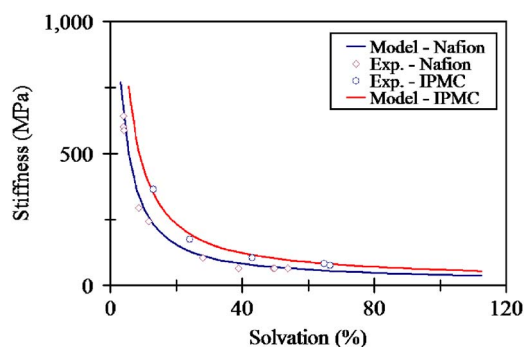


FIG. 7. Uniaxial stiffness (Young's modulus) of bare Nafion 117 and IPMC (data points and the solid curve, model) in Na<sup>+</sup>-form vs solvation; glycerol as solvent.

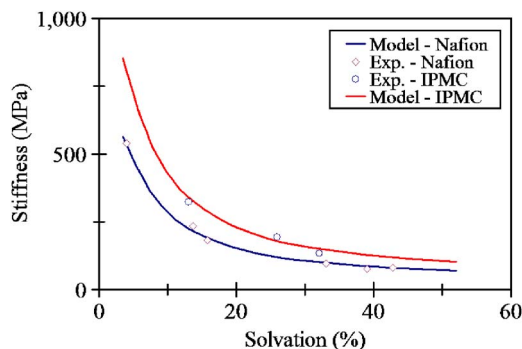


FIG. 11. Uniaxial stiffness (Young's modulus) of bare Nafion 117 and IPMC (data points and the solid curve, model) in K<sup>+</sup>-form vs solvation; glycerol as solvent.

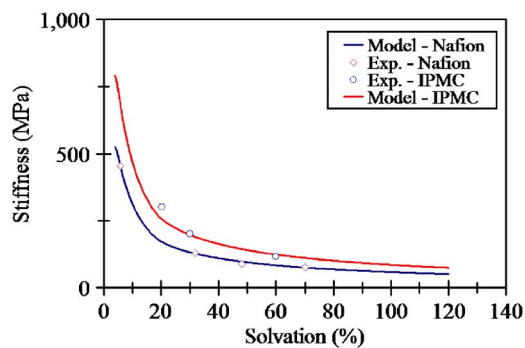


FIG. 8. Uniaxial stiffness (Young's modulus) of bare Nafion 117 and IPMC (data points and the solid curve, model) in Na<sup>+</sup>-form vs solvation; 15-Crown-5 as solvent.

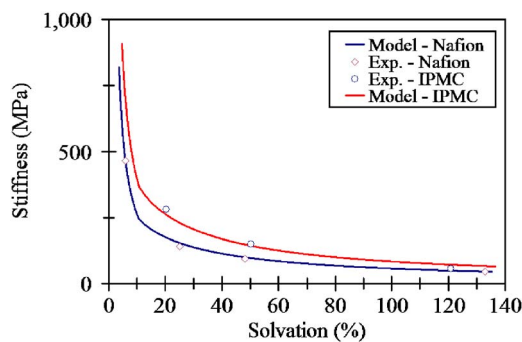


FIG. 12. Uniaxial stiffness (Young's modulus) of bare Nafion 117 and IPMC (data points and the solid curve, model) in K<sup>+</sup>-form vs solvation; 15-Crown-5 as solvent.

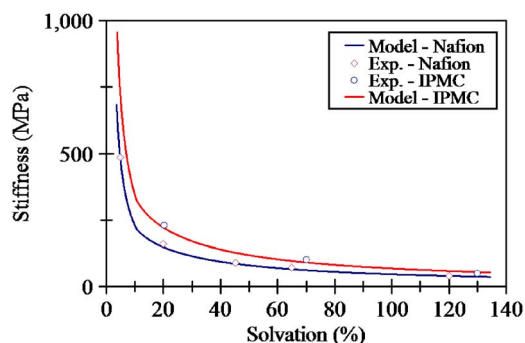


FIG. 9. Uniaxial stiffness (Young's modulus) of bare Nafion 117 and IPMC (data points and the solid curve, model) in Na<sup>+</sup>-form vs solvation; 18-Crown-6 as solvent.

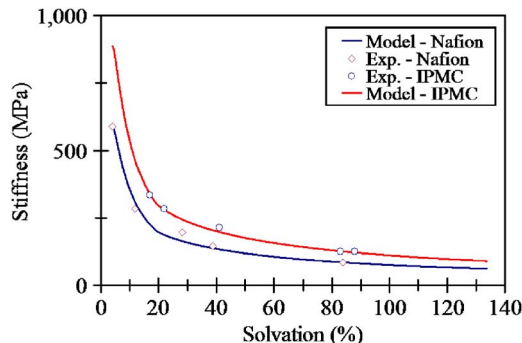


FIG. 13. Uniaxial stiffness (Young's modulus) of bare Nafion 117 and IPMC (data points and the solid curve, model) in K<sup>+</sup>-form vs solvation; 18-Crown-6 as solvent.

## IV. IPMC ACTUATION

### A. Tip displacement

We assume that, in response to changes in the cluster's effective pressure, the solvent will diffuse into and out of the clusters until the elastic resistance of the matrix polymer in the boundary layers balances the internal cluster pressure. The resulting strains are called *eigenstrains*. For a cantilevered sample in pure bending, the radius of curvature  $R_b$  is related to the maximum bending strain  $\varepsilon_{\max}$  by

$$\varepsilon_{\max} \approx \pm \frac{H}{R_b}, \quad (24)$$

where  $H$  is half of the IPMC sample thickness (see Fig. 14).

The volumetric strain  $\varepsilon_v$  is given by

$$\varepsilon_v = \ln[1 + w(x, t)]. \quad (25)$$

Relating the bending due to the volumetric strain to the bending resistance of the sample, the radius of curvature  $R_b$  as a measure of actuation, becomes

$$\frac{L}{R_b} = \frac{L}{2H^3(3\bar{Y}_{\text{IPMC}} - 2Y_B)} \int_{-h}^h Y_{\text{BL}}[w(x, t)]x \times \ln[1 + w(x, t)]dx, \quad (26)$$

where  $h$  is the thickness of the bare ionomer,  $L$  is the cantilever's length,  $Y_{\text{BL}}[w(x, t)]$  is the boundary layer's Young's modulus,  $x$  measures the distance along the cross section of the strip from its midpoint, as shown in Fig. 14, and a strip of unit width is considered.

### B. Voltage-induced cation redistribution

The redistribution of cations under an applied potential is modeled using the coupled electrochemical equations that characterize the net flux of the species, caused by the electrochemical potentials (chemical concentration and electric field gradients). The total flux consists of cation migration and solvent transport. Cation migration is assumed to occur first, followed by the diffusion-controlled solvent transport. The flux  $J_i$  of species  $i$  is characterized by<sup>10-12</sup>

$$J_i = -\frac{C_i D_i}{RT} \frac{\partial \mu_i}{\partial x} + C_i v_i, \quad (27)$$

where  $D_i$  is the diffusivity coefficient,  $\mu_i$  is the chemical potential,  $C_i$  is the concentration, and  $v_i$  is the velocity of species  $i$ . The chemical potential is defined by

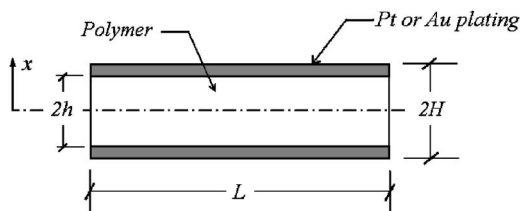


FIG. 14. Schematic of the cross section of an IPMC.

$$\mu_i = \mu_0 + RT \ln(\gamma_i C_i) + z_i \phi F, \quad (28)$$

where  $\mu_0$  is the reference chemical potential,  $\gamma_i$  is the affinity of species  $i$ ,  $z_i$  is the species charge, and  $\phi$  is the electric potential. We assume an ideal solution where  $\gamma_i = 1$  and, since there is only one type of cation, drop the subscript  $i$  and rewrite (27) as

$$J = -D \frac{\partial C}{\partial x} - \frac{z D C F}{RT} \frac{\partial \phi}{\partial x} + C v, \quad (29)$$

where  $D$ ,  $C$ , and  $z$  are the ionic diffusivity coefficient, concentration, and charge of the cations, respectively. The variation in the electric potential field,  $\phi = \phi(x, t)$ , in the membrane is governed by the basic Poisson electrostatic equations,<sup>13,14</sup>

$$\frac{\partial(\kappa E)}{\partial x} = z(C - C^-)F, \quad E = -\frac{\partial \phi}{\partial x}, \quad (30)$$

where  $E$  and  $\kappa$  are the electric field and the electric permittivity, respectively. Now, since the solvent velocity is very small, we may neglect the last term in (29) and, in view of (30) and continuity, obtain

$$J(x, t) = -D \left[ \frac{\partial C(x, t)}{\partial x} - z C(x, t) \left( \frac{F}{RT} \right) E(x, t) \right], \quad (31)$$

$$\frac{\partial C(x, t)}{\partial t} = -\frac{\partial J(x, t)}{\partial x}, \quad (32)$$

$$\frac{\partial E(x, t)}{\partial x} = z \left( \frac{F}{\bar{\kappa}} \right) [C(x, t) - C^-]. \quad (33)$$

Here  $\bar{\kappa}$  is the overall electric permittivity of the solvated IPMC sample that can be estimated from its measured effective capacitance. The above system of equations can be directly solved numerically, or they can be solved analytically using approximations. In the following sections, both methods are considered and the results are presented and compared.

### 1. Finite-difference solution of cation transport

An efficient finite-difference simulation procedure for the solution of the steady-state and transient versions of the Nernst-Planck and Poisson system of equations is used, following Brumleve and Buck.<sup>3</sup> This allows for both spatial and temporal variations. The resulting implicit and nonlinear equations are solved using an iterative Newton-Raphson technique.<sup>15</sup> Equations (31), (32), and (3) are converted into finite-difference form as follows:

$$J_j = -D \left[ \frac{C_{j+1} - C_j}{\Delta X M_j} - z \frac{C_{j+1} + C_j}{2} \left( \frac{F}{RT} \right) E_j \right], \quad (34)$$

$$1 \leq j \leq N-1,$$

$$C_j - C_j^0 = -\frac{\Delta t}{\Delta X B_j} (J_j - J_{j-1}), \quad 1 \leq j \leq N, \quad (35)$$

$$\frac{\partial E_j}{\partial x} = z \frac{F}{\bar{\kappa}} (C_j - C^-), \quad 1 \leq j \leq N, \quad (36)$$

$$\Delta t = t_{k+1} - t_k, \quad \Delta XB_1 = \frac{x_2}{2}, \quad \Delta XB_N = \frac{x_N - x_{N-1}}{2},$$

$$\Delta XM_j = x_{j+1} - x_j, \quad 1 \leq j \leq N-1, \quad (37)$$

$$\Delta XB_j = \frac{x_{j+1} - x_{j-1}}{2}, \quad 2 \leq j \leq N-1,$$

$N$  = total number of spatial elements.

The physical parameters in Eqs. (34)–(36) are rendered dimensionless as follows:

$$X = x/\ell, \quad t' = tD/\ell^2, \quad C(x,t) = C(x,t)/C^-,$$

$$\phi'(x,t) = \phi(x,t)F/IRT, \quad K = \bar{\kappa}RT/C^- \ell^2 F^2, \quad (38)$$

where the length  $\ell$  is defined later on by Eqs. (45). Substituting (34) in (35) and using (30) to relate the electric field to the electric potential, we obtain

$$C_1 - C_1^0 - \frac{\Delta t'}{\Delta XB_1} \left[ \left( \frac{C_2 - C_1}{\Delta XM_1} - z \frac{C_2 + C_1}{2} \frac{\phi'_2 - \phi'_1}{\Delta XM_1} \right) \right] = 0, \quad (39)$$

$j = 1,$

$$C_j - C_j^0 - \frac{\Delta t'}{\Delta XB_j} \left\{ \frac{C_{j+1} - C_j}{\Delta XM_j} - \frac{C_j - C_{j-1}}{\Delta XM_{j-1}} - \frac{z}{2} \left[ (C_{j+1} + C_j) \right. \right. \\ \left. \left. \times \left( \frac{\phi'_{j+1} - \phi'_j}{\Delta XM_j} \right) + (C_j + C_{j-1}) \left( \frac{\phi'_j - \phi'_{j-1}}{\Delta XM_{j-1}} \right) \right] \right\} = 0, \quad (40)$$

$2 \leq j \leq N-1,$

$$C_N - C_N^0 - \frac{\Delta t'}{\Delta XB_N} \left[ - \left( \frac{C_N - C_{N-1}}{\Delta XM_1} \right. \right. \\ \left. \left. - z \frac{C_N + C_{N-1}}{2} \frac{\phi'_N - \phi'_{N-1}}{\Delta XM_{N-1}} \right) \right] = 0, \quad j = N, \quad (41)$$

$$\left( \frac{\phi'_{j+1} - \phi'_j}{\Delta XM_j} \right) - \left( \frac{\phi'_j - \phi'_{j-1}}{\Delta XM_{j-1}} \right) - \frac{K}{\Delta XM_j} [z(C_j - 1)] = 0, \quad (42)$$

$2 \leq j \leq N-1.$

To improve efficiency, the resulting equations are solved using smaller time steps  $\Delta t'$  at the start of the actuation, and larger  $\Delta t'$  at later times. Similarly, smaller grid spacing is used close to the electrodes, and larger ones near the center of the membrane. The values of the ion concentration and the electric potential are defined at the center of the grids (separated by  $\Delta XB$ ), while those of the electric field are defined at their boundaries (separated by  $\Delta XB$ ). The finite-difference spatial mesh is illustrated in Fig. 15. To simulate the transient response, very small time steps are used.

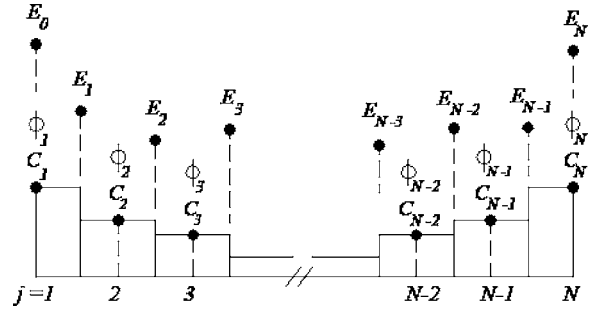


FIG. 15. Typical simulation grid showing the location of the concentration, electric potential, and electric field;  $E_0$ ,  $\phi_1$ , and  $C_1$  are defined at the left interface, and  $E_N$ ,  $\phi_N$ , and  $C_N$  at the right interface. Throughout the rest of the grid, the concentration and electric potential are defined at the center of each volume element and electric fields are defined at its boundaries.

Equations (39) and (41) guarantee zero cation flux into and out of the membrane. Also, the electric potential at the two ends are prescribed by

$$\phi_1 = -(\varphi_0/2), \quad \phi_N = (\varphi_0/2), \quad (43)$$

where  $\varphi_0$  is the applied potential. To apply the Newton-Raphson method to the problem at hand, we recast Eqs. (39)–(42) in the following difference form:

$$a_j = - \frac{\Delta t'}{\Delta XB_j} \left[ \frac{1}{\Delta XM_j} - z \left( \frac{\phi'_j - \phi'_{j-1}}{\Delta XM_{j-1}} \right) \right], \quad 2 \leq j \leq N,$$

$$b_j = 1 + \frac{\Delta t'}{\Delta XB_j} \left[ \left( \frac{1}{\Delta XM_j} + \frac{1}{\Delta XM_{j-1}} \right) - \frac{z}{2} \left( \frac{\phi'_{j+1} - \phi'_j}{\Delta XM_j} \right. \right. \\ \left. \left. - \frac{\phi'_j - \phi'_{j-1}}{\Delta XM_{j-1}} \right) \right], \quad 2 \leq j \leq N-1,$$

$$c_j = \frac{\Delta t'}{\Delta XB_j} \left[ - \frac{z}{2} \left( \frac{\phi'_{j+1} - \phi'_j}{\Delta XM_j} \right) - \frac{1}{\Delta XM_j} \right], \quad 1 \leq j \leq N-1,$$

$$d_j = - \frac{\Delta t'}{\Delta XB_j} \left[ z \left( \frac{C_j + C_{j-1}}{\Delta XM_{j-1}} \right) \right], \quad 3 \leq j \leq N,$$

$$f_j = - \frac{\Delta t'}{\Delta XB_j} \left[ z \left( \frac{C_{j+1} + C_j}{\Delta XM_j} \right) \right], \quad 3 \leq j \leq N,$$

$$y_j = - \frac{K}{\Delta XM_j} \left( \frac{1}{\Delta XM_j} + \frac{1}{\Delta XM_{j-1}} \right), \quad 2 \leq j \leq N-1,$$

$$x_j = z, \quad 2 \leq j \leq N-1,$$

$$s_j = \frac{K}{\Delta XM_j} \left( \frac{1}{\Delta XM_{j-1}} \right), \quad 3 \leq j \leq N-1,$$

$$w_j = \frac{K}{\Delta XM_j} \left( \frac{1}{\Delta XM_j} \right), \quad 2 \leq j \leq N-1,$$

$$t_j = \frac{\Delta t'}{\Delta XB_j} \left[ z \left( \frac{C_{j+1} + C_j}{\Delta XM_j} + \frac{C_j + C_{j-1}}{\Delta XM_{j-1}} \right) \right], \quad 2 \leq j \leq N-1,$$

$$g_1 = C_1^* - C_1^0 - \frac{1}{\Delta XB_1} \left[ \Delta t' \left( \frac{C_2^* - C_1^*}{\Delta XM_1} - z \frac{C_2^* + C_1^*}{2} \frac{\phi_2^* - \phi_1^*}{\Delta XM_1} \right) \right], \quad j = 1,$$

$$g_j = C_j^* - C_j^0 - \frac{\Delta t'}{\Delta XB_j} \left\{ \frac{C_{j+1}^* - C_j^*}{\Delta XM_j} - \frac{C_j^* - C_{j-1}^*}{\Delta XM_{j-1}} - \frac{z}{2} \left[ (C_{j+1}^* + C_j^*) \left( \frac{\phi_{j+1}^* - \phi_j^*}{\Delta XM_j} \right) + (C_j^* + C_{j-1}^*) \left( \frac{\phi_j^* - \phi_{j-1}^*}{\Delta XM_{j-1}} \right) \right] \right\},$$

$$2 \leq j \leq N - 1,$$

$$g_N = C_N^* - C_N^0 - \frac{1}{\Delta XB_N} \left[ \Delta t' \left( \frac{C_N^* - C_{N-1}^*}{\Delta XM_{N-1}} - z \frac{C_N^* + C_{N-1}^*}{2} \frac{\phi_N^* - \phi_{N-1}^*}{\Delta XM_{N-1}} \right) \right], \quad j = N,$$

$$h_j = \frac{K}{\Delta XM_j} \left[ \left( \frac{\phi_{j+1}^* - \phi_j^*}{\Delta XM_j} \right) - \left( \frac{\phi_j^* - \phi_{j-1}^*}{\Delta XM_{j-1}} \right) + z(C_j^* - 1) \right], \quad 2 \leq j \leq N - 1. \quad (44)$$

The results for the cation transfer for a Nafion-based IPMC in Li<sup>+</sup>-form and with water as the solvent, under a dc electric potential  $\varphi_0$  of 1.25 V are shown in Figs. 16 and 17, which show the variation of the normalized charge density  $Q(x, t)$ ,  $Q(x, t) = [C(x, t)/C^-] - 1$ , through the thickness of the IPMC sample at indicated instants. In the simulation, it is assumed that  $\Delta XM_j = \Delta XB_j$ ,  $j = 2, 3, \dots, N - 1$ , and 40 elements are used within 1/7 of the sample thickness at each end. For the rest of the ionomer cross section close to the center, we have used 40 elements. For the time steps, we have used 1 ms for  $t < IT$  and 1 s thereafter until the steady-state solution is reached; for the simulation results that are discussed in what follows,  $IT = 150$  has been used.

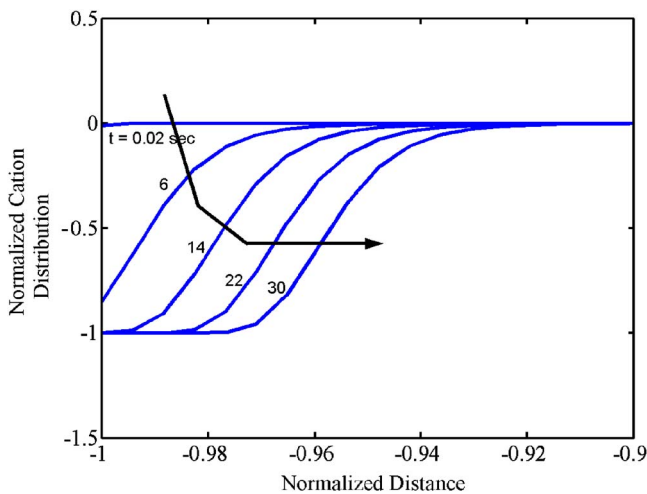


FIG. 16. Anode boundary layer cation depletion over time; Nafion-based IPMC in Li<sup>+</sup>-form with water as solvent, 1.25 V dc electric potential.

The results suggest that the boundary layers initially form antisymmetrically, and then become nonsymmetric. The anode boundary layer forms gradually, although the time scale for this formation is small (0.25 s for the example discussed). This matches the experimental results shown in Fig. 18. The effective permittivity  $\bar{\kappa}$  is calculated to be 0.0269 F/m, based on the measured effective capacitance of 11.9 mF/cm<sup>2</sup>, and  $C^-$  is calculated to be 1185 mol/m<sup>3</sup>, based on the solvent uptake of 53% for the bare ionomer.

Nemat-Nasser and Li<sup>5</sup> assumed an antisymmetric cation distribution along the sample and showed that it then must have the following form:

$$C(x) = C^- + \frac{\bar{\kappa}\varphi_0}{2F\ell^2 \sinh(h/\ell)} \sinh(x/\ell), \quad \ell = \left( \frac{\bar{\kappa}RT}{C^-F^2} \right)^{1/2}. \quad (45)$$

Nemat-Nasser<sup>2</sup> has shown that the final steady-state cation distribution is not antisymmetric, but, rather, it is completely nonsymmetric. Numerical results show that the cation distribution along the sample starts from an antisymmetric solution, but it then becomes nonsymmetric as the cations of the clusters in the anode boundary layer are depleted.

**2. Approximate solution with one time scale**

Ignoring small terms in Eqs. (31)–(33) we obtain the following expression:<sup>2</sup>

$$\frac{\partial}{\partial x} \left\{ \frac{\partial(\kappa E)}{\partial t} - D \left[ \frac{\partial^2(\kappa E)}{\partial x^2} - \frac{C^- F^2}{\kappa RT} (\kappa E) \right] \right\} = 0. \quad (46)$$

This equation provides a natural length scale  $\ell$  defined by (45), and a natural time scale  $\tau$  given by

$$\tau = \frac{\ell^2}{D}. \quad (47)$$

The final (equilibrium) length of the anode boundary layer that is completely depleted of its cations is given by

$$\ell' = \left( \sqrt{\frac{2\varphi_0 F}{RT}} - 2 \right) \ell. \quad (48)$$

Nemat-Nasser<sup>2</sup> shows that the final (equilibrium) cation concentration, the electric field, and the electric potential within the anode boundary layer,  $-h < x \leq -h + \ell'$ , are given by

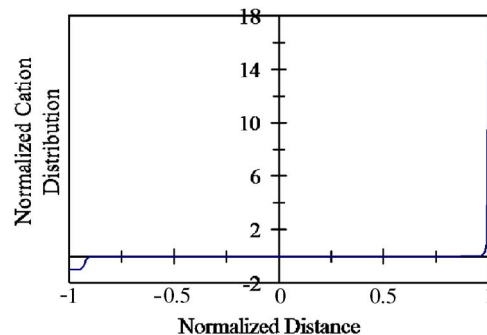


FIG. 17. Numerical results for the anode and cathode cation distributions at equilibrium; Nafion-based IPMC in Li<sup>+</sup>-form with water as solvent, 1.25 V dc electric potential.

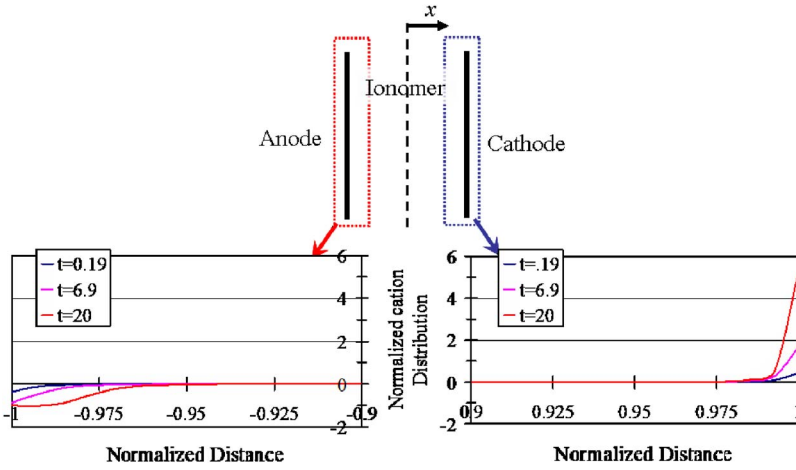


FIG. 18. Numerical results for the anode and cathode boundary layer formation; Nafion-based IPMC in Li<sup>+</sup>-form with water as solvent, 1.25 V dc electric potential.

$$C = 0, \quad E^{(1)}(x) = \frac{1}{\ell} \left( -K_0 \frac{x}{\ell} + E_0 \right),$$

$$\phi^{(1)}(x) = K_0 \left( \frac{x}{\ell} \right)^2 - E_0 \frac{x}{\ell} + A_0, \tag{49}$$

$$K_0 = \frac{C^- F \ell^2}{\bar{\kappa}} = \frac{RT}{F}.$$

Similarly, in the cathode boundary layer,  $-h + \ell' < x \leq h$ , Nemat-Nasser<sup>2</sup> has obtained

$$E^{(2)}(x) = \frac{1}{\ell} \left[ B_0 \exp\left(\frac{x}{\ell}\right) + B_1 \exp\left(-\frac{x}{\ell}\right) \right],$$

$$\phi^{(2)}(x) = -B_0 \exp(x/\ell) + B_1 \exp(-x/\ell) + B_2, \tag{50}$$

$$\frac{C(x) - C^-}{C^-} = \frac{F}{RT} \left[ B_0 \exp\left(\frac{x}{\ell}\right) - B_1 \exp\left(-\frac{x}{\ell}\right) \right],$$

where  $E_0, A_0, B_0, B_1$ , and  $B_2$  are the integration constants, to be fixed using the boundary and continuity conditions, leading to the following expressions:

$$E_0 = K_0(1 - a'), \quad A_0 = \frac{\varphi_0}{2} - K_0 \left( 1 + \frac{\ell'}{\ell} - 2a \right),$$

$$B_0 = \exp(-a) \left[ \frac{\varphi_0}{2} + B_1 \exp(-a) + B_2 \right], \tag{51}$$

$$B_1 = K_0 \exp(-a'),$$

$$B_2 = \frac{\varphi_0}{2} - \frac{1}{2} K_0 \left[ \left( 1 + \frac{\ell'}{\ell} \right)^2 + 1 \right],$$

where  $a \equiv h/\ell$  and  $a' \equiv h'/\ell$  are generally very small. Using this fact, the above constants are obtained from the following boundary conditions:

$$C(-h') = 0, \quad h' = h - \ell', \quad E^{(1)}(-h') = E^{(2)}(-h'), \tag{52}$$

$$\phi^{(1)}(-h') = \phi^{(2)}(-h'), \quad \int_{-h}^h [C(x,t) - C^-] dx = 0.$$

As an example, the equilibrium charge distribution across the Nafion-based IPMC in Li<sup>+</sup>-form with water as the solvent, under a dc electric potential  $\varphi_0 = 1.25$  V and after 300 s, using the approximate solution (ignoring small terms) is shown in Fig. 19. This distribution is attained gradually over time. Thus, it is necessary to also estimate the temporal charge variation. Nemat-Nasser<sup>2</sup> shows that, with good accuracy, the (equilibrium) spatial variation of the charge distribution can be modified to include the temporal effect using the following form:

$$\frac{C(x) - C^-}{C^-} = g(t) \left[ \frac{F}{RT} \left( B_0 \exp\left(\frac{x}{\ell}\right) - B_1 \exp\left(-\frac{x}{\ell}\right) \right) \right], \tag{53}$$

$$g(t) = 1 - \exp(-t/\tau).$$

### 3. Approximate solution with two time scales

The approximate solution with one time scale can be improved by introducing a second time scale. To this end, we start with the basic Eq. (46) and assume that the solution is antisymmetric in a period less than, say,  $\tau_1$ , given by

$$E(x) = \frac{1}{\ell} \left[ B_0 \exp\left(\frac{x}{\ell}\right) + B_1 \exp\left(-\frac{x}{\ell}\right) \right], \quad E = -\frac{\partial \phi}{\partial x},$$

$$\phi(-h) = (\varphi_0/2), \quad \phi(h) = -(\varphi_0/2), \tag{54}$$

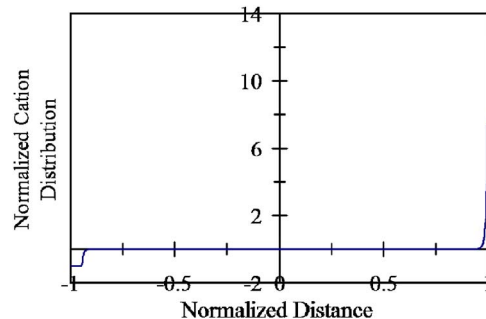


FIG. 19. Variation of the normalized charge density,  $Q(x,t)$ , through the thickness of a Nafion-based IPMC in Li<sup>+</sup>-form with water as solvent; with  $a \equiv h/\ell = 136$ , and  $\varphi_0 = 1.25$  V.

$$\int_{-h}^h [C(x,t) - C^-] dx = 0,$$

where, in view of the boundary conditions (54), we also have

$$B_0 = B_1 = \frac{\varphi_0}{2} \exp(-a). \quad (55)$$

Now, we assume that for times greater than  $\tau_1$ , the anode boundary layer growth is governed by

$$\frac{\ell'(t)}{\ell} = \sqrt{\frac{2\phi_0'(t)F}{RT}} - 2, \quad (56)$$

where the function  $\phi_0'(t)$  is chosen to have the following form:

$$\phi_0'(t) = \varphi_0 \left[ 1 - \exp\left(-\frac{t - \tau_1}{\tau_2}\right) \right] \quad (57)$$

based on the numerical results and experimental observations. Then, the final solution becomes

$$\frac{C(x,t) - C^-}{C^-} = \frac{F}{RT} [B_0(t)\exp(x/\ell) - B_1(t)\exp(-x/\ell)],$$

$$B_0(t) = \exp(-a) \left[ \frac{\phi_0'(t)}{2} + B_1 \exp(-a) + B_2(t) \right], \quad (58)$$

$$B_1 = K_0 \exp(-a'),$$

$$B_2(t) = \frac{\phi_0'(t)}{2} - \frac{1}{2} K_0 \left\{ \left[ 1 + \frac{\ell'(t)}{\ell} \right]^2 + 1 \right\},$$

where  $B_0(t)$ ,  $B_1(t)$ , and  $B_2(t)$  are time-dependent parameters resulting from the spatial integration of the basic equations.

The results of the accumulated charge in the cathode boundary layer for various approaches are presented and compared with the experimental results in Fig. 20. As is seen, the numerical results and the results of the approximate solution with two time scales nicely fit the experimental data. We used  $\tau_1 = 0.25$  s and  $\tau_2 = 6$  s in the two-time-scale approach to obtain the results shown in Fig. 20.

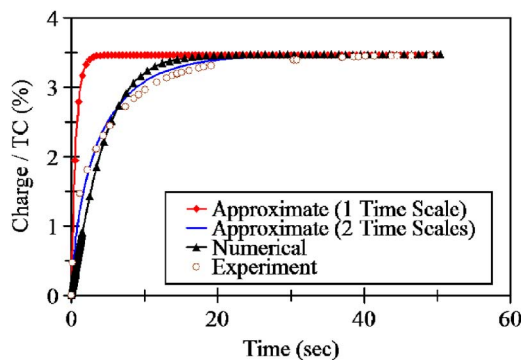


FIG. 20. Comparison between various approaches for the solution of cation transport over time; Nafion-based IPMC in  $\text{Li}^+$ -form with water as solvent; 1.25 V dc electric potential.

## C. Boundary layers

As stated, the application of an electric potential produces two thin boundary layers, one near the anode and the other near the cathode electrodes, while maintaining the overall electric neutrality in the IPMC strip. The cation imbalance within the clusters of each boundary layer changes the osmotic, electrostatic, and elastic forces that tend to expand or contract the corresponding clusters, forcing the solvents out of or into the clusters, and produces the bending motion of the cantilever. Therefore, in this model, the volume fraction of the solvent within each boundary layer is assumed to be controlled by the effective pressure in the corresponding clusters produced by the osmotic, electrostatic, and elastic forces. These forces cause the cathode boundary layer to contract during the back relaxation, expelling the extra solvents onto the IPMC's surface, while cations continue to accumulate within the cathode boundary layer. This, in fact, is what we have observed in open air during the very slow back relaxation of IPMCs that are solvated with ethylene glycol and, particularly, with glycerol.

### 1. Anode boundary layer

At equilibrium state, the total *effective* anode boundary layer length  $L_A$  is given by

$$L_A \equiv \ell + \ell' = \left( \sqrt{\frac{2\varphi_0 F}{RT}} - 1 \right) \ell. \quad (59)$$

The normalized total ion (cation and anion) concentration within each boundary layer is

$$\nu(x,t) = \frac{C(x,t)}{C^-} + 1. \quad (60)$$

The osmotic pressure then is

$$\Pi(x,t) = \frac{\phi Q_B^- K_0}{w(x,t)} \nu(x,t). \quad (61)$$

As the anode boundary layer is being depleted of its cations, electrostatic interaction forces develop among the remaining fixed anions, introducing an additional pressure, say,  $p_{AA}$ , within the cluster, while at the same time, the dipole-dipole interaction forces,  $p_{ADD}$ , are being diminished. The two effects are coupled, since the cation distribution within a cluster would depend on its concentration. Nemat-Nasser<sup>2</sup> has simplified the required analysis by assuming that the two effects are uncoupled. We follow the same approach here to calculate  $p_{AA}$ , arriving at

$$p_{AA}(x,t) = \frac{1}{18\kappa(x,t)} Q_B^{-2} \frac{R_0^2}{[w(x,t)]^{4/3}} \left[ -\frac{C(x,t)}{C^-} + 1 \right], \quad (62)$$

where  $\kappa(x,t)$  is the effective electric permittivity of the clusters and  $R_0$  is the initial (dry) cluster size; for the definition and derivation of various parameters, see Nemat-Nasser.<sup>2</sup> Similarly, the corresponding  $p_{ADD}$  is estimated from

$$p_{\text{ADD}}(x,t) = \frac{1}{3\kappa(x,t)} Q_B^{-2} \left[ \frac{\alpha(x,t)}{w(x,t)} \right]^2 \left[ \frac{C(x,t)}{C^-} \right]. \quad (63)$$

The total pressure within a typical anode boundary layer cluster hence is

$$p_c(x,t) = \Pi(x,t) + p_{\text{AA}}(x,t) + p_{\text{ADD}}(x,t). \quad (64)$$

## 2. Cathode boundary layer

Consider now the clusters within the cathode boundary layer. Unlike the anode boundary layer, the clusters in the cathode boundary layer are filled with additional cations. The distribution of cations inside the cathode boundary layer is not uniform. The normalized total ion concentration and the osmotic pressure within the cathode boundary layer are defined by (60) and (61).

In the cathode boundary layer, we identify two forms of electrostatic interaction forces. One is repulsion due to the cation-anion pseudodipoles already present in the clusters, and the other is due to the extra cations that migrate into the clusters and interact with the existing pseudodipoles. The additional stresses produced by this latter effect may tend to expand or contract the clusters, depending on the distribution of cations relative to fixed anions. We again model each effect separately, although in actuality they are coupled. The dipole-dipole interaction pressure in the cathode boundary layer clusters is estimated as follows

$$p_{\text{CDD}}(x,t) = \frac{1}{3\kappa(x,t)} Q_B^{-2} \left[ \frac{\alpha(x,t)}{w(x,t)} \right]^2 \frac{C^-}{C(x,t)}. \quad (65)$$

We represent the interaction between the preexisting dipoles and the additional cations that move into a cluster under the action of an applied voltage, by dipole-cation interaction stresses defined by

$$p_{\text{DC}}(x,t) = \frac{2Q_B^{-2}}{9\kappa(x,t)} \frac{R_0\alpha(x,t)}{[w(x,t)]^{5/3}} \left[ \frac{C(x,t)}{C^-} - 1 \right]. \quad (66)$$

For sulfonates in Nafion-based IPMCs, we expect extensive restructuring and redistribution of the extra cations. It appears that this process underpins the observed reverse relaxation of the Nafion-based IPMC strip. In fact, this redistribution of the cations within clusters in the cathode boundary layer may quickly diminish the value of  $p_{\text{DC}}$  to zero or even render it negative. To represent this, Eq. (66) is modified by a relaxation factor  $g_1(t)$  and rewritten as

$$p_{\text{DC}}(x,t) = \frac{2Q_B^{-2}}{9\kappa(x,t)} \frac{R_0\alpha(x,t)}{[w(x,t)]^{5/3}} \left[ \frac{C(x,t)}{C^-} - 1 \right] g_1(t), \quad (67)$$

$$g_1(t) = [r_0 + (1 - r_0)\exp(-t/\tau')], \quad r_0 < 1,$$

where  $\tau'$  is the relaxation time and  $r_0$  is the equilibrium fraction of the dipole-cation interaction forces. In this approximation,  $r_0$  can be negative, since under the action of additional cations within a cluster, a rearrangement in the effective polarity of the dipoles can be induced. In the case of ethylene glycol and glycerol,  $r_0$  is negative; see Tables VII–IX.

The total pressure inside the cathode boundary layer cluster hence is

$$p_c(x,t) = \Pi(x,t) + p_{\text{DC}}(x,t) + p_{\text{CDD}}(x,t). \quad (68)$$

## D. Variation in solvent uptake

Pressure inside the clusters within the backbone ionomer,  $p_c(x,t)$ , is resisted by the elastic stress  $\sigma_r$  at the cluster boundary  $a_0$ :

$$\sigma_r(a_0,t) = -p_0(t) + K(t) \left[ \frac{w(x,t)}{w_0} \right]^{-4/3}. \quad (69)$$

As a result, the net pressure  $t_c$  on the solvent inside the cluster can be defined as

$$t_c(x,t) = -\sigma_r(a_0,t) + p_c(x,t), \quad (70)$$

where (64) and (68) define the corresponding  $p_c(x,t)$ . The ion flux must satisfy continuity equation (22). For the solvent, we have

$$\frac{\dot{w}(x,t)}{1+w(x,t)} + \frac{\partial v(x,t)}{\partial x} = 0. \quad (71)$$

The solvent exchange in the clusters should be calculated using the diffusion equation and the initial boundary conditions. Since the anode boundary layer is rather thin, we may assume a uniform  $w(x,t)$  and  $t_c$  across this boundary layer. So in the anode and cathode boundary layers, (71) is approximated by

$$\frac{\dot{w}(x,t)}{1+w(x,t)} = D_{\text{BL}} t_c(x,t), \quad (72)$$

where  $D_{\text{BL}}$  is introduced to include the effect of the anode and cathode boundary layer thickness in hydraulic permeability. We have assumed that this value is constant across the anode and cathode boundary layers.

## E. Response upon shorting

Shorting refers to the state when the electric potential is removed and the two faces of the sample are electrically connected. In this case, experiments suggest that some cations transport relatively rapidly into the cation-depleted anode boundary layer, while a fraction of cations within the cation-rich cathode boundary layer transports back into the interior of the IPMC. The remaining extra cations in the cathode boundary layer then move slowly out into the interior region until the equilibrium condition (a uniform charge distribution) is eventually achieved; this may take a rather long time depending on the cations and the nature of the solvent. To model this phase of the actuation, it is assumed that the equations governing the discharge process are similar to those of the charging process, but now we start with a set of initial conditions that characterize the state just prior to shorting.

Assume that the shorting occurs at  $t=T_S$ . We assume that, upon shorting, there is a diffusion of the excess cations from the cathode boundary layer into the interior of the membrane, while cations diffuse back into the anode bound-

ary layer. Eventually this leads to a uniform distribution throughout the membrane's thickness. Thus, in the anode boundary layer we have, for  $t \geq T_S$ ,

$$p_{ADD}(x,t) = \frac{1}{3\kappa(x,t)} Q_B^{-2} \left[ \frac{\alpha(x,t)}{w(x,t)} \right]^2 \frac{C(x,t)}{C^-}, \quad (73)$$

$$p_{AA}(x,t) = \frac{1}{18\kappa(x,t)} Q_B^{-2} \frac{R_0^2}{[w(x,t)]^{4/3}} \left[ 1 - \frac{C(x,t)}{C^-} \right]. \quad (74)$$

The above equations are obtained by simply assuming that the discharge is the reverse of the charging process, although in reality the various involved processes are coupled. In the cathode boundary layer, for  $t \geq T_S$ , we set

$$p_{CDD}(x,t) = \frac{1}{3\kappa(x,t)} Q_B^{-2} \left[ \frac{\alpha(x,t)}{w(x,t)} \right]^2 \frac{C^-}{C(x,t)}, \quad (75)$$

$$p_{DC}(x,t) = \frac{2Q_B^{-2}}{9\kappa(x,t)} \frac{R_0 \alpha(x,t)}{[w(x,t)]^{5/3}} \left[ \frac{C(x,t)}{C^-} - 1 \right] g_1(t), \quad (76)$$

where  $g_1(t)$  is given in (67).

As an example, we summarize the procedure that has been followed to model a Nafion-based IPMC sample in  $\text{Na}^+$ -form with water as the solvent, and subjected to 1.25 V dc potential. Values of  $a_1$  and  $a_2$  are obtained from the stiffness model. The parameter  $R_0$  must be calculated with some care. Since  $w_1 \approx (a_1/R_0)^3$ , where  $w_1$  is the initial volume fraction of the solvent in the Nafion part of the IPMC and  $a_1$  is the cluster size at solvent uptake  $w_1$ , we may set  $R_0 \approx w_1^{-1/3} a_1$ . The cluster size  $a_1$  is estimated from the Gierke cluster size model,<sup>16</sup> as modified by Li and Nemat-Nasser;<sup>17</sup> a summary is given in the Appendix. Guided by that model, a cluster size,  $a_1 = 1.65$  nm, is assumed to exist prior to the application of the potential. Table VI gives the values of various parameters used for the purpose of modeling the actuation response. As discussed earlier, two different time steps are used to reduce the simulation time as noted in Table VI. The free parameters  $r_0$ ,  $\tau'$ ,  $D$ , and  $D_{BL}$  are chosen to fit the data. Depending on the solvent and the cation, both  $D$  and  $D_{BL}$  are expected to decrease with increasing viscosity of the solvent, as they actually do. The measured capacitance also varies over a range even for the same solvent and cation. Thus it may be adjusted to within a reasonable range to fit the data.

TABLE VI. Parameters used for actuation response modeling; Nafion-based IPMC in  $\text{Na}^+$ -form and water as solvent, subjected to a step potential and then shorted.

Parameters	$\text{Na}^+$ -Water
$\Delta t$ (s)	0.001/0.1
$N$	120
$2h$ ( $\mu\text{m}$ )	212
$2H$ ( $\mu\text{m}$ )	224
$L$ (mm)	28.6
$w_1$ (%)	50
$\varphi_0$ (V)	1.25
$a_1$ (nm)	1.65
$r_0$	0.08
$\tau'$ (s)	0.7
$D$ ( $\text{m}^2/\text{s}$ )	$120\ell^2$
$D_{BL}$ ( $\text{m}^2/\text{s}$ )	$2.5 \times 10^{-2}$
Cap ( $\text{F}/\text{m}^2$ )	123

Figure 21(a) shows the charge transfer over time for the strip of Nafion-based IPMC in  $\text{Na}^+$ -form with water, subjected to a 1.25 V step potential for 46.7 s and then shorted. In the figure, the heavy solid curve represents the model and the geometric symbols connected by a solid curve represent the experimental results. The model in this case predicts faster charge transfer than that observed experimentally, as is seen in Fig. 21(a). Figure 21(b) shows the corresponding variation of the normalized curvature with time.

The same procedure is used to model Nafion-based IPMCs in other cation forms with other solvents.<sup>6</sup> For solvents such as glycerol or crown ethers, the sensitivity of our measurement devices was insufficient to discern in certain cases the necessary signals from that of the background noise. So for the purpose of modeling, a value within the measured range is used for the effective capacitance. Tables VII–IX represent various values of the model parameters for Nafion-based IPMCs with indicated cations and solvents. The corresponding actuation graphs are given in Figs. 22–32.

## V. SUMMARY AND CONCLUSIONS

Both the initial relatively fast motion and the subsequent relaxation of Nafion-based IPMCs have been modeled based on the nanoscale mechanisms proposed by Nemat-Nasser.<sup>2</sup> Remarkably, the model correctly produces both qualitatively

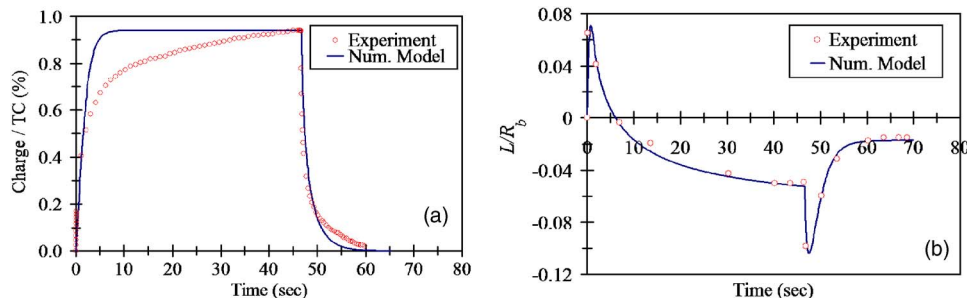


FIG. 21. (a) Charge transfer over time for a strip of Nafion-based IPMC in  $\text{Na}^+$ -form with water, subjected to a 1.25 V step potential; the heavy solid curve is the result of the model and the geometric symbols are experimental results, shorted at 46.7 s. (b) Variation of normalized curvature over time for a strip of Nafion-based IPMC in  $\text{Na}^+$ -form with water, subjected to a 1.25 V step potential; the heavy solid curve is the result of the model and the geometric symbols are experimental results, shorted at 46.7 s.

TABLE VII. Parameters used for actuation response modeling; Nafion-based IPMC in Li<sup>+</sup>-form and various solvents, subjected to a step potential and then shorted.

Parameters	Li <sup>+</sup>		
	Ethylene glycol	Glycerol	12CR4
$\Delta t$ (s)	0.001/1	0.001/5	0.001/10
$N$	120	120	120
$2h$ ( $\mu\text{m}$ )	290	212	285
$2H$ ( $\mu\text{m}$ )	309	232	306
$L$ (mm)	40.4	30.8	38.6
$w_1$ (%)	271	125	145
$\varphi_0$ (V)	1.25	2.0	2.0
$a_1$ (nm)	2.8	1.0	2.0
$r_0$	0.38	-0.2	0.55
$\tau'$ (s)	0.01	0.001	0.1
$D$ (m <sup>2</sup> /s)	$1.2\ell^2$	$0.5\ell^2$	$0.5\ell^2$
$D_{BL}$ (m <sup>2</sup> /s)	$9.0 \times 10^{-3}$	$1.4 \times 10^{-3}$	$6.0 \times 10^{-3}$
Cap (F/m <sup>2</sup> )	120	17	22.0

and, with reasonable accuracy, quantitatively all observed, rather peculiar, behaviors of this class of soft actuators.

First, the stiffness of the bare ionomer and the corresponding IPMC are modeled for each cation form and various degrees of solvation, identifying and evaluating several microstructural parameters that are also necessary for the modeling of the corresponding actuation.

To model the actuation, we assumed that the application of an electric potential produces two boundary layers, one near the anode and the other near the cathode electrodes. As a result, the clusters in the anode boundary layer are gradually depleted of their cations, while those in the cathode boundary layer are gradually supplied with additional cations. Under the influence of these extra cations and because of the strong acidity of the sulfonates, there is a redistribution of the cations within the clusters in the cathode boundary layer that occurs at a rate defined by a time scale  $\tau'$ . This modifies the effective dipole-cation interaction forces, thereby contributing to the back relaxation.

TABLE VIII. Parameters used for actuation response modeling; Nafion-based IPMC in Na<sup>+</sup>-form and various solvents, subjected to a step potential and then shorted.

Parameters	Na <sup>+</sup>			
	Ethylene glycol	Glycerol	15CR5	18CR6
$\Delta t$ (s)	0.001/1	0.001/5	0.001/10	0.001/10
$N$	120	120	120	120
$2h$ ( $\mu\text{m}$ )	290	212	285	248
$2H$ ( $\mu\text{m}$ )	309	232	306	264
$L$ (mm)	40.4	30.8	28.6	28.6
$w_1$ (%)	55	67	181	166
$\varphi_0$ (V)	2.0	2.0	2.0	3.0
$a_1$ (nm)	0.6	1.2	2.8	2.6
$r_0$	-0.1	-0.16	0.22	0.6
$\tau'$ (s)	0.1	0.1	100	0.02
$D$ (m <sup>2</sup> /s)	$10\ell^2$	$0.05\ell^2$	$0.3\ell^2$	$0.03\ell^2$
$D_{BL}$ (m <sup>2</sup> /s)	$9.0 \times 10^{-3}$	$7.0 \times 10^{-3}$	$9.0 \times 10^{-4}$	$1.0 \times 10^{-3}$
Cap (F/m <sup>2</sup> )	55	180	60	150

TABLE IX. Parameters used for actuation response modeling; Nafion-based IPMC in K<sup>+</sup>-form and various solvents, subjected to a step potential and then shorted.

Parameters	K <sup>+</sup>			
	Ethylene glycol	Glycerol	15CR5	18CR6
$\Delta t$ (s)	0.001/5	0.001/5	0.001/10	0.001/1
$N$	120	120	120	120
$2h$ ( $\mu\text{m}$ )	185	185	255	285
$2H$ ( $\mu\text{m}$ )	206	206	274	306
$L$ (mm)	28.6	28.6	34.35	38.6
$w_1$ (%)	45	36	124	145
$\varphi_0$ (V)	1.5	2.0	2.5	3.0
$a_1$ (nm)	0.8	0.5	2.6	3.5
$r_0$	-0.07	-0.2	1.0	1.0
$\tau'$ (s)	0.1	0.1	1.0	10
$D$ (m <sup>2</sup> /s)	$5\ell^2$	$10\ell^2$	$0.01\ell^2$	$0.25\ell^2$
$D_{BL}$ (m <sup>2</sup> /s)	$3.0 \times 10^{-3}$	$7.0 \times 10^{-3}$	$2.0 \times 10^{-4}$	$9.0 \times 10^{-4}$
Cap (F/m <sup>2</sup> )	110	50	40	15

To model the distribution of the cations over the thickness of the IPMC as a function of time, the Nernst equation is used to represent the cation flux. The electrostatics equations are used to account for the electric field within the membrane, and the continuity equations and the necessary boundary conditions are used to ensure charge conservation and consistency with the imposed boundary data.

The cation imbalance within the clusters (but not the IPMC) changes the osmotic, electrostatic, and elastic forces that tend to expand or contract the corresponding clusters, forcing the solvents out of or into the clusters, and produces the bending motion of the cantilever. Therefore, in this model, the volume fraction of the solvent within each boundary layer is assumed to be controlled by the effective pressure in the corresponding clusters produced by the osmotic, electrostatic, and elastic forces. These forces cause the cathode boundary layer to contract during the back relaxation, expelling the extra solvents onto the IPMC's surface while cations continue to accumulate within the cathode boundary layer. This has been actually observed during the very slow back relaxation of IPMCs that are solvated with ethylene glycol and, particularly, with glycerol.

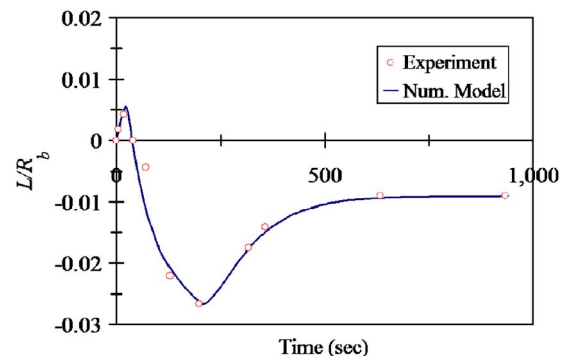


FIG. 22. Variation of normalized curvature over time for a strip of Nafion-based IPMC in Li<sup>+</sup>-form with ethylene glycol (EG), subjected to a 2.0 V step potential; the heavy solid curve is the result of the model and the geometric symbols are experimental results, shorted at 199.2 s.

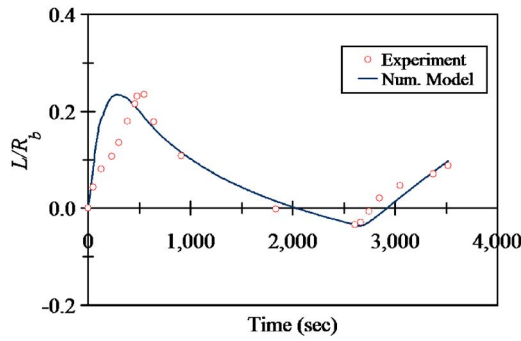


FIG. 23. Variation of normalized curvature over time for a strip of Nafion-based IPMC in  $\text{Li}^+$ -form with glycerol (G), subjected to a 2.0 V step potential; the heavy solid curve is the result of the model and the geometric symbols are experimental results, shorted at 2611.1 s.

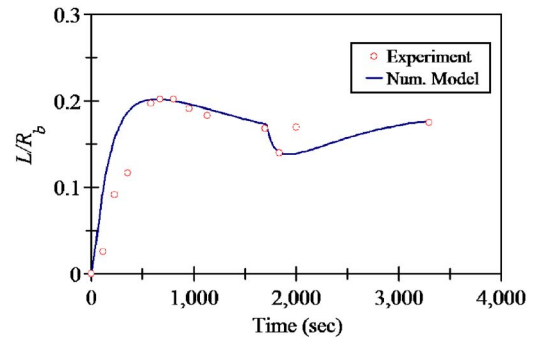


FIG. 27. Variation of normalized curvature over time for a strip of Nafion-based IPMC in  $\text{Na}^+$ -form with 15CR5, subjected to a 2 V step potential; the heavy solid curve is the result of the model and the geometric symbols are experimental results, shorted at 1837.0 s.

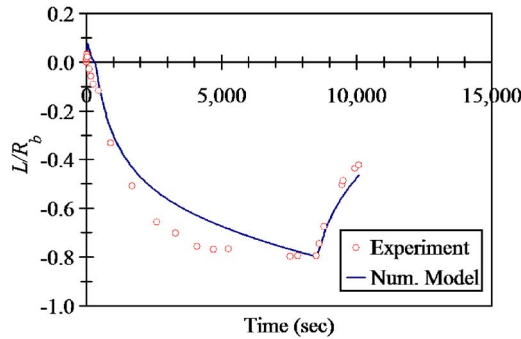


FIG. 24. Variation of normalized curvature over time for a strip of Nafion-based IPMC in  $\text{Li}^+$ -form with 12CR4, subjected to a 2 V step potential; the heavy solid curve is the result of the model and the geometric symbols are experimental results, shorted at 8514.0 s.

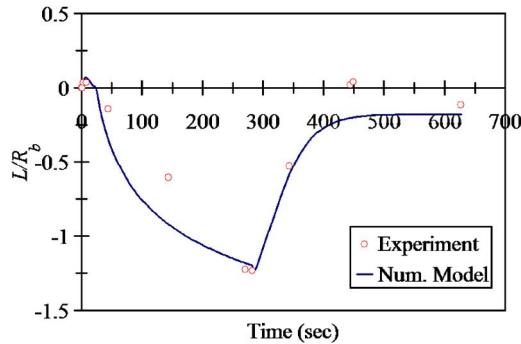


FIG. 25. Variation of normalized curvature over time for a strip of Nafion-based IPMC in  $\text{Na}^+$ -form with ethylene glycol (EG), subjected to a 2.0 V step potential; the heavy solid curve is the result of the model and the geometric symbols are experimental results, shorted at 281.1 s.

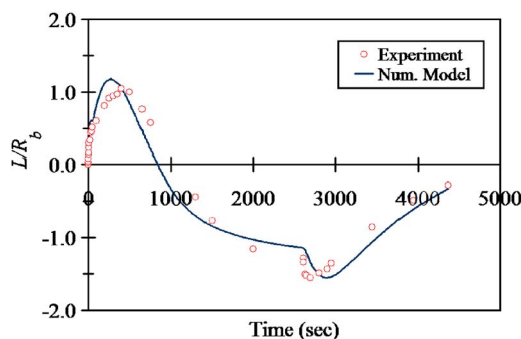


FIG. 26. Variation of normalized curvature over time for a strip of Nafion-based IPMC in  $\text{Na}^+$ -form with glycerol, subjected to a 2 V step potential; the heavy solid curve is the result of the model and the geometric symbols are experimental results, shorted at 2610.0 s.

The coupled equations are solved incrementally. At each step the effective pressures in the anode and cathode clusters are calculated. Then, using the rate form of the continuity equation for the solvent and a linear diffusion equation, the changes in the volume fraction of the solvent in the anode and cathode boundary layers are calculated together with the resulting volumetric strains and hence the increment of the induced bending curvature. The calculations also take into account the dependence of the stiffness of the IPMC on the volume fraction of the solvent that varies along the thickness and in time. To simplify the modeling, this variation is first fitted to a simple power law that closely follows both the measured and modeled values of the stiffness. While this is not necessary, it does lead to a stable numerical calculation procedure.

Based on the model and comparison with the experimental results, the following overall observations are made: (i) The neutralizing cations, the nature and the degree of saturation of the solvent, the electrode morphology, and the chemical structure and characteristics of the backbone polymer are all important parameters that affect the electrical-chemical-mechanical response of IPMCs, both quantitatively and qualitatively. IPMCs with heavier and more viscous solvents have slower actuations, higher solvent uptakes, smaller stiffness at fully solvated states, and lower overall capacitance. (ii) The basic mechanism of the IPMC actuation is governed by the cation transport, which creates imbalance in

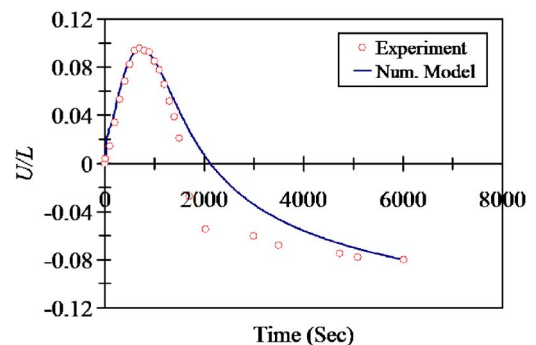


FIG. 28. Variation of normalized displacement over time for a strip of Nafion-based IPMC in  $\text{Na}^+$ -form with 18CR6, subjected to a 3 V step potential; the heavy solid curve is the result of the model and the geometric symbols are experimental results.

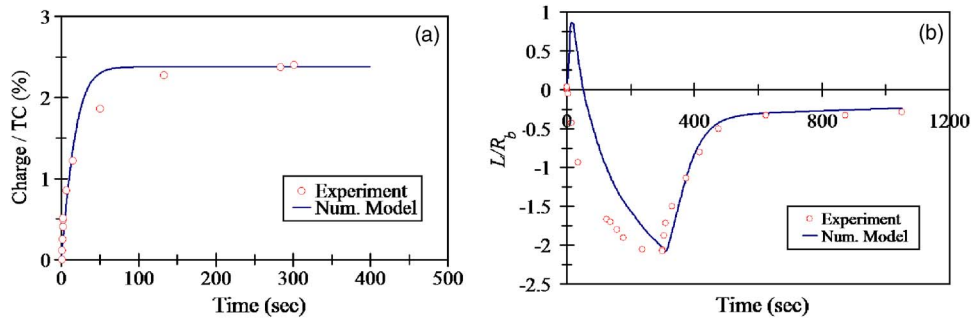


FIG. 29. (a) Variation of accumulated charge over time for a strip of Nafion-based IPMC in  $K^+$ -form with ethylene glycol, subjected to a 1.5 V step potential; the heavy solid curve is the result of the model and the geometric symbols are experimental results, shorted at 300.0 s. (b) Variation of normalized curvature over time for a strip of Nafion-based IPMC in  $K^+$ -form with ethylene glycol (EG), subjected to a 1.5 V step potential; the heavy solid curve is the result of the model and the geometric symbols are experimental results, shorted at 300.0 s.

electrostatic and osmotic pressures within the clusters (while maintaining overall electric neutrality) and hence promotes solvent transport. (iii) The application of an electric potential produces two boundary layers, one near the anode and the other near the cathode electrodes. The clusters in the anode boundary layer are gradually depleted of their cations, while those in the cathode boundary layer are gradually supplied with additional cations. Experimental results such as the ones shown in Figs. 21(a) and 28(a) suggest the continued depletion of cations from the anode and accumulation into the cathode boundary layers long after the initial fast motion and way into the period of back relaxation of the cantilever that is actuated by a dc voltage. (iv) Once equilibrium is reached, most of the clusters in the anode boundary layer are completely depleted of their cations and those in the cathode boundary layer are rich with additional cations. (v) Initially, the variation of the cation density in the cathode and anode boundary layers is centrally symmetric, but once the clusters near the electrodes in the anode boundary layer are depleted of their cations, the length of the anode boundary layer increases as cations move out of its clusters, while cations are added to the clusters in the cathode boundary layer. (vi) For a fully solvated IPMC membrane, the equilibrium distribution of the cations and the internal potential that develops under the action of an applied step potential of magnitude  $\varphi_0$  depend on the effective permittivity  $\bar{\kappa}$ , the ionomer thickness  $h$ , the concentration of the anions  $C^-$ , and the magnitude of

the applied potential  $\varphi_0$ . (vii) The effective length of the anode boundary layer at equilibrium is given by

$$L_A \equiv \ell + \ell' = \left( \sqrt{\frac{2\varphi_0 F}{RT}} - 1 \right) \ell, \quad \ell = \left( \frac{\bar{\kappa} RT}{C^- F^2} \right)^{1/2}.$$

This has been established by Nemat-Nasser<sup>2</sup> using an approximate analytical estimate and is confirmed by our numerical solution. (viii) Nafion-based IPMCs with alkali metals have relatively late and long back relaxation when solvated with ethylene glycol and glycerol; this is true even for Nafion-based IPMCs in  $Li^+$ -form that show minimal back relaxation when hydrated. (ix) Nafion-based IPMCs that are neutralized with alkali metals show remarkably different responses when solvated with crown ethers. In  $Li^+$ -form with 12-Crown-4, the response under a dc potential involves extensive but slow back relaxation, whereas in  $Na^+$ -form with 15-Crown-5, it shows very little back relaxation and, most interestingly, in  $K^+$ -form with 18-Crown-6, there is no back relaxation at all. Moreover, the sample in  $Na^+$ -form with 18-Crown-6 shows extensive back relaxation, whereas in  $K^+$ -form with 15-Crown-5, there is some back relaxation towards the cathode, but this is then reversed and the sample relaxes back towards the anode while still under the dc potential. (x) The variation of the response from sample to sample (or even for the same sample tested at various times) is often so great that only an approximate quantitative correspondence between the theoretical predictions and the ex-

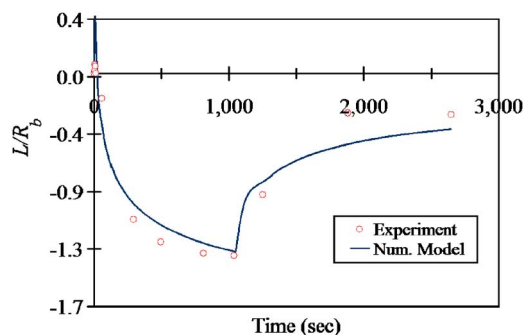


FIG. 30. Variation of normalized curvature over time for a strip of Nafion-based IPMC in  $K^+$ -form with glycerol, subjected to a 2 V step potential; the heavy solid curve is the result of the model and the geometric symbols are experimental results, shorted at 1036.1 s.

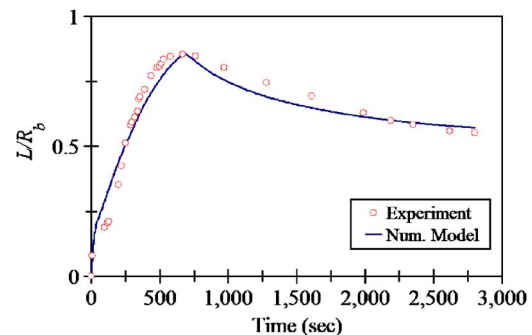


FIG. 31. Variation of normalized curvature over time for a strip of Nafion-based IPMC in  $K^+$ -form with 18CR6, subjected to a 2.5 V step potential; the heavy solid curve is the result of the model and the geometric symbols are experimental results, shorted at 669.0 s.

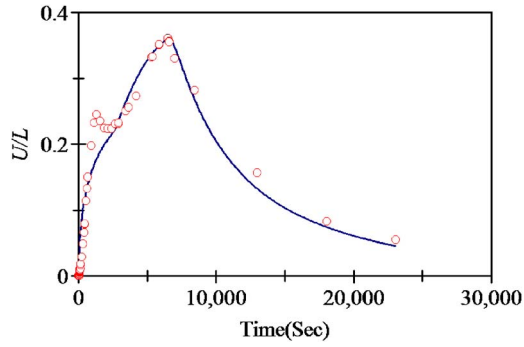


FIG. 32. Variation of normalized displacement over time for a strip of Nafion-based IPMC in K<sup>+</sup>-form with 15CR5, subjected to a 2.5 V step potential; the heavy solid curve is the result of the model and the geometric symbols are experimental results.

perimental results should be expected, or reasonably required. Nevertheless, the model seems to correctly produce, both qualitatively and, with reasonable accuracy, quantitatively, all the observed responses of these IPMCs. (xi) To apply high electric potentials without electrolysis, IPMCs with other solvents such as ethylene glycol, glycerol, and crown ether solutions can be used. This enables actuating a strip of an IPMC in open air for rather long time periods, and/or at low temperatures. (xii) To maximize the normalized curvature of a cantilevered strip with its bending stiffness held fixed, it is necessary to maximize the effective capacitance and surface conductivity of the IPMC.

## ACKNOWLEDGMENTS

The authors wish to thank Dr. Steve Wax (DARPA), Dr. Len Buckley (NRL), Dr. Carlos Sanday (NRL), and Dr. Randy Sands for their initial support of this research at UCSD which has been continued now for a while without external funding at UCSD's CEAM. The authors are grateful to Professor Mohsen Shahinpoor and Dr. K. J. Kim for providing the Nafion-based IPMC samples; to Dr. K. Asaka for providing the Flemion-based IPMC samples; to Dr. Yosi Bar-Cohen for his continued interest and stimulating interaction; to Jon Isaacs and Dave Lischer for developing the experimental equipment and techniques; and to Dr. Jeff McGee for the helpful code used to obtain the effective capacitance. This work has been supported by CEAM of the University of California, San Diego.

## APPENDIX: CLUSTER SIZE APPROXIMATION

X-ray scanning of the Nafion membranes<sup>18</sup> has shown that in the process of solvent absorption, hydrophilic regions consisting of clusters are formed within the membrane. Hydrophilicity and hydrophobicity are generally terms used for affinity or lack of affinity toward the polar molecule of water. In the present work we use these terms for interaction toward any polar solvent (i.e., ethylene glycol). Cluster formation is promoted by the aggregation of hydrophilic ionic sulfonate groups located at the terminus of vinyl ether sulfonate pendants of polytetrafluoroethylene chain. While these regions are hydrophilic, the membrane backbone is hydrophobic and it is believed that the motion of the solvent takes place

among these clusters via the connecting channels. The characteristics of these clusters and channels are important factors in IPMC sample behavior. The size of the solvated cluster radius ( $a_1$ ) depends on the cation form, type of solvent used, and the amount of solvation. The average cluster size can be calculated by minimizing the free energy of the cluster formation with respect to the cluster size. The total energy for cluster formation consists of an elastic ( $U_{ela}$ ), an electrostatic ( $U_{ele}$ ), and a surface ( $U_{sur}$ ) component. The elastic energy is given by<sup>17</sup>

$$U_{ela} = \frac{3NkT}{\langle h^2 \rangle} \left( \sqrt[3]{\frac{NEW_{ion}}{\rho^* N_A}} - a_1 \right)^2, \quad (A1)$$

$$\rho^* = \frac{\rho_B + w\rho_s}{1 + w}, \quad (A2)$$

where  $N$  is the number of dipoles inside a typical cluster,  $k$  is Boltzmann's constant,  $T$  is the temperature,  $\langle h^2 \rangle$  is the mean end-to-end chain length,  $\rho^*$  is the effective density of the solvated membrane, and  $N_A$  is Avogadro's number ( $6.023 \times 10^{23}$ ). The electrostatic energy is defined by

$$U_{ele} = -g \frac{N^2 m^2}{4\pi\kappa_e a_1^3}, \quad (A3)$$

where  $g$  is a geometric factor,  $m$  is the dipole moment, and  $\kappa_e$  is the effective permittivity within the cluster. The surface energy can be expressed as

$$U_{sur} = 4\pi a_1^2 \gamma, \quad (A4)$$

where  $\gamma$  is the surface energy density of the cluster. Therefore, the total energy due to the presence of clusters in the ionomer is given by

$$U_{tot} = n(U_{ele} + U_{ela} + U_{sur}), \quad (A5)$$

where  $n$  is the number of clusters present in the membrane. Minimizing this energy with respect to cluster size, ( $\partial U_{tot}/\partial a_1 = 0$ ), gives the optimum cluster size at which the free energy of the ionomer is minimum. In this manner Li and Nemat-Nasser<sup>17</sup> have obtained

$$a_1 = \left\{ \frac{\gamma \langle h^2 \rangle EW_{ion} (w + \Delta V)}{2RT \rho_B} \times \left[ 1 - \sqrt[3]{\frac{4\pi\rho_B}{3\rho^*(w + \Delta V)}} \right]^{-2} \right\}^{1/3}, \quad (A6)$$

$$\Delta V = \frac{N_A V_i \rho_d}{EW_{ion}}, \quad (A7)$$

where  $V_i$  is the volume of a single ion exchange site. Assuming that  $\langle h^2 \rangle = EW_{ion}\beta$ ,<sup>19</sup> it can be seen that

$$a_1^3 = \frac{\gamma\beta}{2RT} \eta, \quad (A8)$$

$$\eta = \frac{EW_{ion}^2 (w + \Delta V)}{\rho_B} \left[ 1 - \sqrt[3]{\frac{4\pi\rho_B}{3\rho^*(w + \Delta V)}} \right]^{-2}. \quad (A9)$$

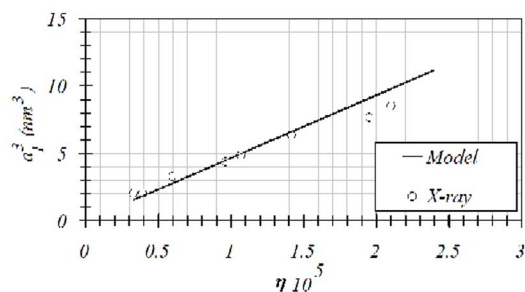


FIG. 33. Cluster size in Nafion membranes with different solvent uptakes.

Figure 33 shows the variation of the cluster size ( $a_1^3$  in  $\text{nm}^3$ ) for different solvent uptakes. Data from Nafion-based IPMC samples with different cations and different solvent uptakes are considered. The model is compared with the experimental results on the cluster size based on x-ray scanning, shown as circles in Fig. 33 for a Nafion ionomer in various cation forms and with water as solvent.<sup>18</sup> We have set  $\beta=1.547$ ,  $\gamma=0.15$ , and  $V_i=68 \times 10^{-24} \text{ cm}^3$  to calculate the cluster size.<sup>19</sup>

As can be seen from Fig. 33, cluster size varies *linearly* with  $\eta$  for different solvents and cation forms. For the Nafion membrane treated with various other considered solvents, we have used the physical properties of the sample prior to the application of a potential and have estimated the cluster size that is needed for modeling the corresponding IPMC actuation.

<sup>1</sup>Y. Bar-Cohen, S. P. Leary, M. Shahinpoor, J. S. Harrison, and J. Smith, Proc. SPIE **3669**, 51 (1999).

<sup>2</sup>S. Nemat-Nasser, J. Appl. Phys. **92**, 2899 (2002).

<sup>3</sup>T. R. Brumleve and R. P. Buck, J. Electroanal. Chem. Interfacial Electrochem. **90**, 1 (1978).

<sup>4</sup>S. Nemat-Nasser and C. Thomas, in *Electroactive Polymer (EAP) Actuators as Artificial Muscles: Reality, Potential and Challenges*, edited by Y. Bar-Cohen, (SPIE, Bellingham, WA, 2001), Chap. 6, pp. 139–191.

<sup>5</sup>S. Nemat-Nasser and J. Y. Li, J. Appl. Phys. **87**, 3321 (2000).

<sup>6</sup>S. Nemat-Nasser, S. Zamani, and Y. Tor, J. Appl. Phys. **99**, 104902 (2006).

<sup>7</sup>S. Nemat-Nasser and Y. Wu, J. Appl. Phys. **93**, 5255 (2003).

<sup>8</sup>J. B. Hasted, D. M. Ritson, and C. H. Collie, J. Chem. Phys. **16**, 1 (1948).

<sup>9</sup>D. R. Lide, *CRC Handbook of Chemistry and Physics*, (CRC, Boca Raton, FL, 2003).

<sup>10</sup>J. O'M. Bockris and A. K. N. Reddy, *Modern Electrochemistry 1: Ionics* (Plenum New York, 1998).

<sup>11</sup>P. Shewmon, *Diffusion in Solids*, 2nd ed. (Minerals, Metals, and Materials Society, Warrendale, PA, 1989).

<sup>12</sup>M. Eikerling, Y. I. Kharkats, A. A. Kornyshev, and Y. M. Volfkovich, J. Electrochem. Soc. **145**, 8 (1998).

<sup>13</sup>J. D. Jackson, *Classical Electrodynamics*, (Wiley, New York, 1962).

<sup>14</sup>W. B. Cheston, *Elementary Theory of Electric and Magnetic Fields* (Wiley, New York, 1964).

<sup>15</sup>B. Carnahan, H. A. Luther, and J. O. Wilkes, *Applied Numerical Methods* (Wiley, New York, 1969).

<sup>16</sup>T. D. Gierke and W. Y. Hsu, ACS Symp. Ser. **180**, 283 (1982).

<sup>17</sup>J. Y. Li and S. Nemat-Nasser, Mech. Mater. **32**, 303 (2000).

<sup>18</sup>T. D. Gierke, C. E. Munn, and P. N. Walmsley, J. Polym. Sci., Polym. Phys. Ed. **19**, 1687 (1981).

<sup>19</sup>W. A. Forsman, Macromolecules **15**, 1032 (1982).